2005

Detailed geochronology of the Mississippi Sound during the late Holocene

Brian Velardo
Louisiana State University and Agricultural and Mechanical College

DETAILED GEOCHRONOLOGY OF THE MISSISSIPPI SOUND DURING THE LATE HOLOCENE

A Thesis

Submitted to the Graduate Faculty of the
Louisiana State University and
Agricultural and Mechanical College
in partial fulfillment of the
requirements for the degree of
Master of Science

in

The Department of Oceanography and Coastal Sciences

by
Brian Velardo
B.S. Louisiana State University and
Agricultural and Mechanical College
at Baton Rouge, 2001

May 2005

Acknowledgments

First and foremost, I would like to thank Dr. Sam Bentley for his patience, kindness, support, and encouragement. I would like to thank each member of my committee, Dr. Jaye Cable, Dr. Harry Roberts, Dr. Gregory Stone, and Dr. Yoko Furukawa for allowing me the opportunity to learn from their collective wealth of knowledge.

I would like to thank all of those who have helped make this a very enjoyable experience and for the sacrifice of blood, sweat, but luckily no tears on the day trips and cruises and for assistance in the lab: Kristi Rotondo, Luke Patterson, Triniti Dufrene, Zahid Muhammad, Will Vienne, Steven Chan, Chris Dauterive, Lindsay Olinde, and the 2002 LSU Geologic Oceanography class.

Floyd DeMers and his guidance in core collection and processing, and the intimate details of wine making were instrumental in helping me progress through this process. I would also like to thank all of the technicians and students in the CSI shop for their patience and assistance, and the captains and crews of the RV Kit Jones, RV Tommy Munro, RV Hermes, and the RV Mcllwain.

Finally, to my family and friends who have been most supportive during the past few years. There was never a discouraging word, but only full support and encouragement. To my parents, you are both examples of what the pursuit of happiness can bring and have taught me to live with integrity and perseverance in the face of tough challenges. Thank You.

Support for this project was provided by the Office of Naval Research, the National Science Foundation, and National Sea Grant.

Table of Contents

Abstract

The Mississippi Sound is a bar-built estuary that parallels the Mississippi Coast. It is bounded on the west by the St. Bernard lobe of the Mississippi River delta, Mobile Bay to the east, and the Gulf Coast barrier islands to the south. Few studies have investigated the late Holocene history of Mississippi Sound. In the present study, historical deposition in the Sound has been investigated using core data collected throughout the western, central, and eastern Mississippi Sound.

The sediments within Mississippi Sound compose a complex depositional system that have responded to changes in sea level and hydrodynamics. Two factors that influence the wave dynamics within Mississippi Sound are changes in water depth and exposure to the open Gulf of Mexico. Decreases in water depths have an inverse relationship to the shear velocity produced by waves. Thus, by decreasing water depth from 3 m to 2.5 m, the shear velocity ($\mathbf{U}_*$), produced from a wave with H = 0.9 m and T = 4 s, would increase from ~0.006 m/s to 0.008 m/s. These changes may be recorded in the sedimentary fabric as changes in the sedimentary facies from a low-energy muddy facies to a higher-energy sandy facies. However, increased exposure to the open Gulf of Mexico allows for larger deep-water waves to impact the Sound. Therefore, by exposing Mississippi Sound to increased wave energy from the Gulf of Mexico, conditions become favorable for the deposition of the higher-energy sandy facies in the deeper water of Mississippi Sound. The sedimentary fabric and geochronology data of recent deposition suggest that physical processes actively rework the sediment in the top 5 cm of the sea-bed; however, biological processes continuously rework the sediment to a depth of 10-12 cm resulting in the destruction of most of the physical stratification. Tropical cyclones impact the sedimentary fabric

such that they are recorded as sandy event beds within a muddy matrix. Approximately 8-26% of the sediment column was deposited by recordable storm events in the Western Mississippi Sound, whereas smaller storm events and typical estuarine processes deposited the other 74 – 92% of the sediment column.

Introduction

The objective of this study is to evaluate the sedimentary processes within Mississippi Sound, and to gain a better understanding of how the system evolved during the Late Holocene. In order to achieve this goal, establishment of sedimentary facies was determined using sedimentological characteristics, and interpretations of depositional environments were made through an investigation into the hydrodynamics of present day depositional environments. Influences of tropical cyclones were also investigated to determine the impact that these storms have on the sedimentary record. While several stratigraphic and geomorphic studies have been conducted in other areas of the Gulf Coast such as the Louisiana and Texas coasts, few studies have investigated the depositional history and processes of sediment deposition within Mississippi Sound. This research will provide incites into the deposition of sediments within Mississippi Sound and may be used in conjunction with other recent studies of late Holocene deposition in the northern Gulf of Mexico to help develop a more comprehensive Holocene history of the northern Gulf of Mexico.

Several sedimentological studies of the surficial sediments of Mississippi Sound conducted throughout the Sound determined that higher concentrations of sandy sediments were present along the coastal beaches and barrier islands, while the more central regions of the sound consisted of higher concentrations of muddy sediments (Priddy, 1955; Upshaw et al., 1966; Isphording and Lamb, 1980, and Chastain, 1981). Chastain (1981) also identified an influx of shelf sands into the Sound occurs through the barrier island passes.

Rainwater (1963) described the geologic history of Mississippi Sound through a coring study along a transect from Beauvoir, Mississippi to Ship Island. Otvos (1975, 1976, 1982, 1985,

1986) described the coastal geology of Louisiana, Mississippi, and Alabama. Otvos' (1985, 1986) investigated Pleistocene and Holocene sediments; however, the studies did not define in detail the Holocene facies of Mississippi Sound. More recently, Otvos and Giardino (2004) studied the evolution of the St. Bernard delta and its influences on western Mississippi Sound.

Hummel and Parker (1995) utilized seismic and core data to identify sedimentary facies and distribution throughout eastern Mississippi Sound. The authors identified seven lithofacies ad inferred depositional environments from their descriptions. Integration of this data with radiometric dates allowed for the calculation of sediment accumulation rates and for the creation of an inundation history for eastern Mississippi Sound.

Cipriani and Stone (2001) studied the net longshore transport and textural changes of the southwest Alabama and Mississippi barrier islands. The authors defined six distinct transport cells characterized by net westward littoral sediment transport within Dauphin Island, Alabama and West Ship Island.

Bentley et al. (2000, 2002) and Keen et al. (2004) investigated the record of event sedimentation within Mississippi Sound the origin and preservation of Hurricane beds in Mississippi Sound through core analysis and numerical modeling of wind, wave, and currents generated by tropical cyclones. A numerical model of storm deposition was employed to predict storm deposition and tested through analysis of cores in Mississippi Sound.

Regional Geologic Setting

The Mississippi coastal zone is part of a large interdeltaic province, which has experienced relatively slow subsidence and deposition of terrigenous clastic sediments since the early Cenozoic time (Rainwater, 1963). However, during the Lower and early Upper Cretaceous, this area was covered by a shallow epicontinental sea and experienced large delta-building

events. A coastal sea covered today's southern Mississippi during the middle and late Eocene and early Oligocene. During regressive stages of the late Paleocene, lower Eocene, and Miocene, the Mississippi shoreline was south of its present location. The Pliocene is not well defined around coastal Mississippi and it is likely represented by an unconformity with Pleistocene sediments overlying late Miocene deposits (Rainwater, 1963).

During the Sangamon interglacial period, about 100,000 yrs BP, the northern Gulf of Mexico was subject to a marine transgression. The onset of the Wisconsin glaciation lowered sea level and the shoreline receded south of the present-day barrier island system (Rainwater, 1963). The maximum late Wisconsin lowstand of sea level was 120-125 m below present and occurred between 20,000 and 17,000 B.P., at the last glacial episode (Curray, 1965). The Holocene Transgression, which followed the Wisconsin glaciation, is characterized by a rapid rise in sea level, greater than 100 m in less than 20,000 years (Curray, 1965). Sea level continued a rapid rise until ~7,000 B.P., when sea level was approximately 10 m below present. By some estimates, during the past 7,000 years, sea level has slowly risen to near its present level (Curray, 1965). It is generally believed that sea level reached near its present level at about 5,000 to 2,500 yr B.P. (Rainwater, 1963). At lower sea stands older deposits were exposed to erosion and weathering. As sea level rose, marine sediments were deposited on the erosional surface. This deposition created a boundary, which made it possible to identify the Pleistocene / Holocene unconformity (Rainwater, 1963).

The chain of barrier islands separating Mississippi Sound from the open Gulf of Mexico was formed during the Holocene Transgression. Otvos (1970) determined that the barrier islands were formed through the emergence of submarine shoals, which were nourished with sediments deposited by littoral drift and currents. Possible sources of sand for the barrier islands are: 1) the

erosion of pre-Holocene headlands along the Alabama-Florida coasts, and 2) the re-working of sediments deposited on the inner continental shelf (Cipriani and Stone, 2001), and 3) input of new sediment from the mainland.

Study Area: Hydrography and Sediments

Mississippi Sound is a bar-built estuary located in the Northern Gulf of Mexico along the Mississippi Gulf coast (Fig. 1). The Sound has an area of approximately 2100 km^2, bounded by Mobile Bay to the east and the St. Bernard lobe of the Mississippi River delta to the west (Eleuterius, 1978). The northern boundary is defined by the state of Mississippi coastal plain, while a barrier island chain (Cat Island, East and West Ship Island, Horn Island, Petit Bois Island, and Dauphin Island) located 10 to 20 km south of the mainland defines the southern boundary of the Sound. The average depth of Mississippi Sound is 2-5 m except for locally deeper troughs near the islands and inlets in the southern portion. In this diurnal micro-tidal environment (~ 0.5 m), a westward long shore current results in westward littoral drift of sediments along the barrier islands (Cipriani and Stone, 2001). Currents are strongest in and near the inlets between the barrier islands (Upshaw et al, 1966). The influx of rivers creates a salinity gradient within the Sound, with the lowest salinities in creek and river mouths to 20 to 25 in broader areas of the Sound (Priddy et al., 1955). Mississippi Sound may become nearly fresh during rainfall events; however, during low rainfall salinity may increase to 35 parts per thousand as Gulf of Mexico water enters the Sound through deep tidal channels (Priddy et al., 1955; Upshaw et. al., 1966). Mississippi Sound is a predominantly well-mixed estuary; however, it may display characteristics of being partially mixed and in highly localized areas it may become stratified (Eleuterius, 1977)

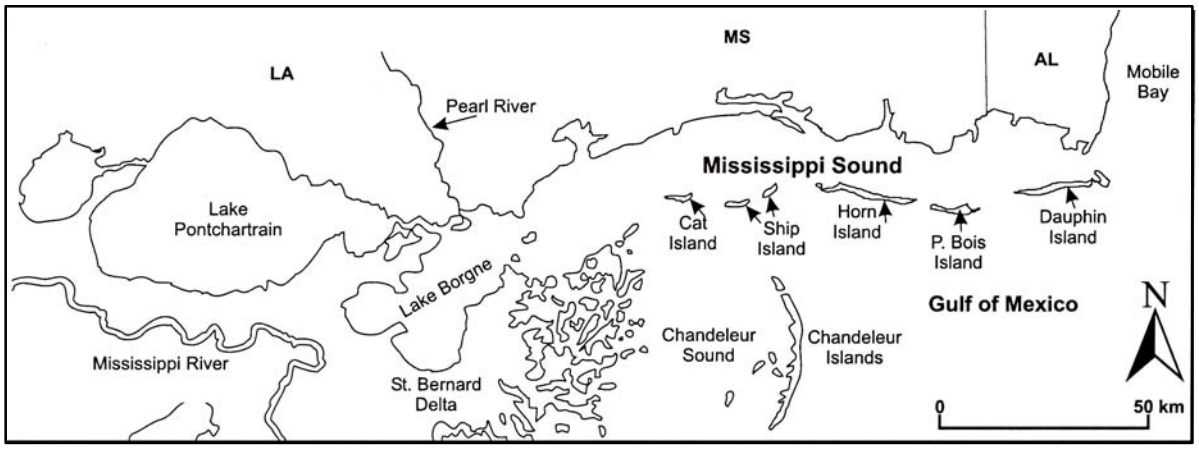

Figure 1. Map of the Mississippi Sound and the surrounding area (adapted from Otvos, 2004)

Primary sources of sediment include the Mississippi River, Mobile River, Pascagoula River, and the Pearl River (Upshaw et al., 1966). Smaller rivers also flow into Mississippi Sound through estuaries and bays. These rivers include the Biloxi and Tchouticabouffa Rivers that flow into Back Bay of Biloxi, and the Jordan and Wolf Rivers flowing into St. Louis Bay. The majority of sediments deposited in the Sound probably have sources in the Appalachians Mountains, and are characteristic of the Eastern Gulf Province. However, a study of clay minerals shows a westward increase in smectite + illite / kaolinite ratios, more characteristic of sediments associated with the Mississippi River than of the Eastern Gulf Province (Milne and Shott, 1958; and Upshaw, 1966; Otvos, 1973). Coarse sediments in Mississippi Sound are mostly orthoquartzitic, but also contain minerals typical of the Eastern Gulf Province. The heavy mineral assemblage of the Eastern Gulf Province is composed mainly of metamorphic mineral suites high in kyanite, epidote, tourmaline, zircon, sillimanite, and rutile. In contrast, Mississippi River sediments commonly contain igneous minerals such as amphibole, pyroxene, epidote, ilmenite, and biotite, an assemblage more typical of the western end of the Sound (Priddy et al., 1955; Upshaw, 1966; Otvos, 1973).

Ludwick (1964) determined that the seabed of Mississippi Sound is predominantly sandy mud, but regions of clean sand occur near the passes and between the islands. Upshaw et al. (1966) found the sediments in the central portion of the Sound to be silt and clay (less than 62μm), with local occurrences of very fine and fine sands (62 – 250 μm). Medium grained sands (greater than 250 μm) occur south of Pascagoula (Upshaw, et al 1966), and coarse-grained sands are found along the barrier islands. A muddy trough occurs between eight and fourteen km south of Gulfport, and from five to eight km south of Bellefontaine Point, north of the eastern tip of Horn Island. Sediments in this trough are 80-98 % mud (Otvos, 1976, Upshaw et al, 1966).

Otvos (1973) described mixed mud-sand areas west of Cat Island, between eastern Horn Island and Pascagoula, and between Biloxi Bay and Dog Key Pass.

Early estimates of sediment thickness indicated a Holocene thickness of 1 to 4 m thick; however, more recent data, including cores and chirp subbottom profiles (Rucker et al., 1990) indicate a much more variable thickness of Holocene sediments, up to 10 m, implying the existence of a more extensive and complex Holocene stratigraphic record, and a more complex Pleistocene surface. In addition to an incomplete understanding of the Holocene sediment record, deposition rates are variable based on where cores are collected and methods used to make estimates. Ludwick (1964) calculated a sediment accumulation rate of ~0.024 cm yr^{-1} from his estimated Holocene thickness. Rainwater (1963) has estimated that since sea level approached its present level about 5000 years ago, about one half of the volume of Mississippi Sound (which he estimated to have an original unfilled depth of 9 m) has been filled, and he calculated an accumulation rate of ~0.122 cm yr^{-1}. Hummell and Parker (1995) calculated an average Holocene sedimentation rate of 0.045 cm yr^{-1}. Bentley et al. (2002) calculated short-term accumulation rates between 0.29 cm yr^{-1} and 0.47 cm yr^{-1}.

Impacts of Tropical Systems

The Northern Gulf of Mexico is frequently impacted by tropical systems of varying strength. In a span of 116 years (1871 to 1986) the northern Gulf Coast has experienced 139 tropical cyclones. Fifty-three of these systems evolved into hurricanes (Neumann et al., 1988). Over a one 100-year period (1900 to 2000), the state of Louisiana and Key West, Florida ranked highest in the frequency of category 3 or stronger hurricane strikes for the coastline from Texas to North Carolina (Muller and Stone, 2001). The role of tropical systems in coastal processes is significant in the stratigraphic record and storms should be regarded as episodic events, which

are important geologic agents of coastal change (Kahn, 1978). Bentley et al. (2000) conducted a study on the preservation potential of event sedimentation within Mississippi Sound, and they determined that ~50% of the net sedimentation within the study area during the past 50 to 100 years was the direct result of event sedimentation from Hurricane Camille in 1969 and an unnamed Hurricane in 1947.

Methods

Gravity cores and box cores were collected from the R/V Kit Jones in western Mississippi Sound in June of 2001. Box cores were also collected on October 11, 2002, one week after Hurricane Lili impacted the western Louisiana coastline, along a transect from the northern margin of the Sound to the south of Horn Island. Vibracores were collected on a cruise on the R/V Tommy Munro in May 2003 (see table 1; Figure 2).

Box Cores

Box cores were sub-sampled for radiochemical analyses, X-radiography, and physical properties. A 10-cm internal diameter PVC pipe was inserted into the sediment and extruded in 2-cm intervals for grain size, porosity, and radiochemistry. Grain size analysis of wet sediment was conducted using a Micromeritics ET-5100 Sedigraph (Coakley and Syvitski, 1991). Samples were sieved at 63 μm and dried to determine the weight percent of sand and mud. A second sample was sieved at 250 μm to separate the coarse fraction, and then the fine fraction was dispersed in one part 0.05% sodium metaphosphate and one part glycerin prior to analysis. Selected cores greater than 50% sand were analyzed using a settling column. Settling column samples were sieved at 63 μm to separate the sand fraction from the sample, and then dried. Samples with abundant shells were sieved with a 200 mm mesh to remove large shells from the sample. A 1 to 2 g sample of the dried sand was then analyzed with the settling column (McCave and Syvitski, 1991).

Slabs for X-radiography were collected by inserting 3-sided Plexiglas trays into the sediment, then sliding the fourth side into place in order to minimize sediment disturbance. The trays were sealed with neoprene plugs to prevent slumping and desiccation before they were brought back to Louisiana State University. In the laboratory, they were x-rayed using a portable

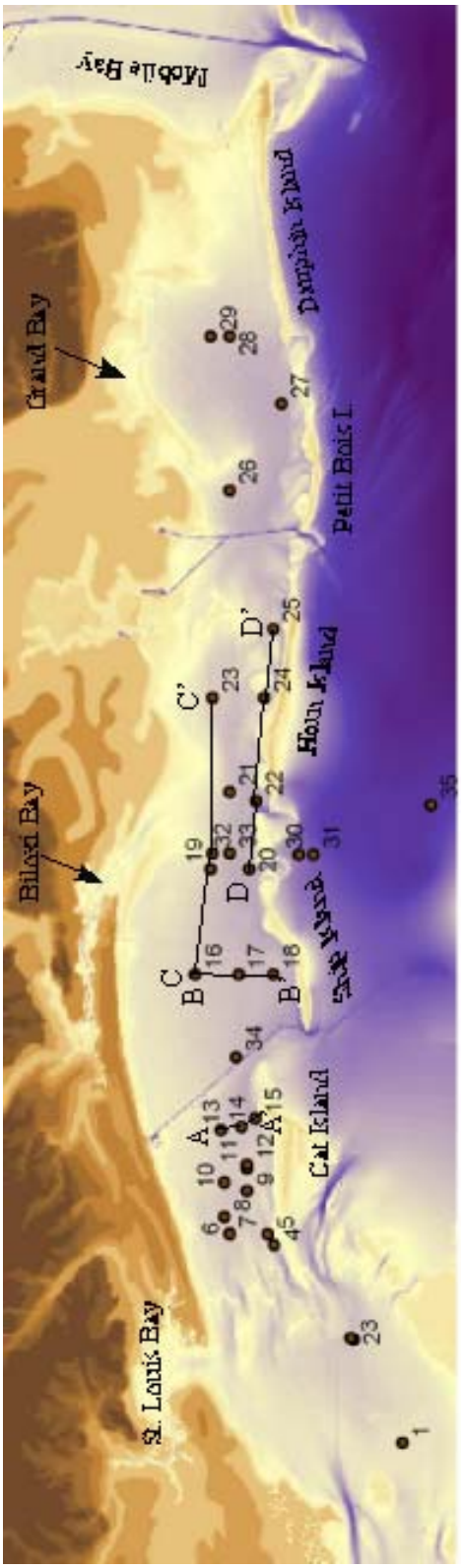

Figure 2. Bathymetric map of Mississippi Sound. Numbers on the map correlate to locations listed on Table 1.

Table 1. Location for map in figure 2

	Core ID	Lattitude	Longitude
1	KJ0601 GC9	30 07' 01.92'' N	89 23' 03.84'' W
2	KJ0601 BC6	30 09' 53.28'' N	89 17' 04.92'' W
3	KJ0601 GC10	30 10' 01.56'' N	89 17' 00.24'' W
4	KJ0601 BC14	30 14' 27.24'' N	89 11' 39.12'' W
5	TM0503 VC31	30 14' 48.00'' N	89 11' 00.00'' W
6	KJ0601 BC3	30 17' 00.60'' N	89 10' 57.72'' W
7	KJ0601 GC11A, B, C	30 16' 59.52'' N	89 10' 59.52'' W
8	TM0503 VC30	30 17' 18.00'' N	89 10' 00.00'' W
9	KJ0601 BC1	30 16' 00.00'' N	89 08' 05.00'' W
10	TM0503 VC29	31 17' 18.00'' N	89 08' 00.00'' W
11	KJ0601 BC12	30 16' 00.12'' N	89 07' 12.00'' W
12	KJ0601 GC12	30 15' 59.76'' N	89 15' 59.76'' W
13	TM0503 VC28	30 17' 30.00'' N	89 04' 60.00'' W
14	TM0503 VC27	30 16' 18.00'' N	89 04' 48.00'' W
15	TM0503 VC26	30 15' 31.97'' N	89 04' 19.57'' W
16	TM0503 VC14	30 18' 60.00'' N	88 56' 00.00'' W
17	TM0503 VC13	30 16' 30.00'' N	88 56' 00.00'' W
18	TM0503 VC12	30 14' 30.00'' N	88 56' 00.00'' W
19	TM0503 VC25	30 18' 06.00'' N	88 49' 54.00'' W
20	TM0503 VC24	30 15' 54.00'' N	88 49' 54.00'' W
21	TM0503 VC1	30 16' 58.80'' N	88 45' 25.58'' W
22	TM0503 VC2	30 15' 29.03'' N	88 45' 58.06'' W
23	TM0503 VC11	30 18' 00.00'' N	88 40' 00.00'' W
24	TM0503 VC10	30 15' 00.00'' N	88 40' 00.00'' W
25	TM0503 VC9	30 14' 30.00'' N	88 35' 60.00'' W
26	TM0503 VC15	30 17' 00.00'' N	88 28' 00.00'' W
27	TM0503 VC16	30 14' 00.00'' N	88 23' 00.00'' W
28	TM0503 VC17	30 17' 00.00'' N	88 19' 06.00'' W
29	TM0503 VC18	30 18' 06.00'' N	88 19' 06.00'' W
30	Shelf 2	30 13' 00.66'' N	88 49' 03.84'' W
31	Shelf 3	30 12' 11.04'' N	88 49' 02.94'' W
32	Estuary 2	30 18' 00.00'' N	88 48' 60.00'' W
33	Estuary 3	30 17' 00.00'' N	88 49' 00.00'' W
34	WAVCIS CSI-13	30 15' 58.20'' N	89 00' 27.00'' W
35	NDBC 42007	30 46' 12.00'' N	88 46' 12.00'' W

veterinary X-ray unit within 5 days of collection. X-radiographs were then digitized for analysis of sedimentary structures.

Gravity and Vibracores

Gravity and vibracores were analyzed using a GEOTEK Multi-Sensor Core Logger (MSCL). Gamma density was measured with a narrow beam of gamma rays emitted from a 10 milli-curie ^{137}Cs source with energies principally at 661 KeV. An ultrasonic P-wave system measured P-Wave speed at 500 kHz. The gravity cores were also analyzed for magnetic susceptibility and electrical resistivity. Magnetic susceptibility was measured through a Bartington Magnetic Loop Sensor. Electrical resistivity was measured through a Non-Contacting Resistivity (NCR) sensor developed by GEOTEK. Selected cores were then split for x-radiography and sub-sampled in 2 cm intervals for grain size, porosity, and radiochemistry.

Radionuclide Geochemistry and Analysis

Sediments were analyzed for ^{137}Cs, ^{210}Pb, and ^{7}Be. Particle reactive radionuclides, such as ^{7}Be ($t_{1/2}$ = 53.3 d) and ^{210}Pb ($t_{1/2}$ = 22.3 yrs) have proven to be effective tools in tracing the depositional processes in coastal zones (Nittrouer et al., 1979; Feng et al., 1999; Sommerfield et al., 1999), and can be used to trace recent sediment accumulation and mixing rates from seasonal to century time scales. Lead-210 is a product of the ^{238}U decay series. Sources of ^{210}Pb in marine sediments include the atmospheric deposition, the decay of ^{226}Ra in the water column or in the sediments, and fluvial delivery. Atmospheric ^{210}Pb is formed through the decay of ^{222}Rn, and is removed by wet and dry deposition. Unsupported ^{210}Pb is the fraction of the detected ^{210}Pb that is absorbed onto marine sediment grain surfaces. Supported ^{210}Pb is formed through the *in situ* decay of ^{222}Rn gas that is produced within sediment grains. Excess ^{210}Pb ($^{210}Pb_{xs}$) is determined by subtracting supported ^{210}Pb from the total ^{210}Pb present in the sediment (Goldberg, 1963;

Appleby and Oldfield, 1978). The anthropogenic radioisotope ^{137}Cs, was first released by the atmospheric testing of hydrogen bombs in 1954, and so can be used as a time marker in the sediment. Because of these characteristics, ^{137}Cs ($t_{1/2}$ =30.7 yrs) can be used to reduce the uncertainty in the results of ^{210}Pb geochronology (Noller, 2000). Longer-lived radioisotopes, such as ^{14}C ($t_{1/2}$ = 5568) can be used to determine fluctuations of a depositional environment over longer timescales (Trumbore, 2000).

The radioisotope ^{7}Be is produced in the Earth's atmosphere by cosmic-ray spallation of nitrogen and oxygen. It becomes associated with aerosols and is transferred to the Earth's surface through both precipitation and dry deposition, where it is quickly scavenged by the sediments and absorbed onto sediments. The ^{7}Be budget for a coastal depositional setting is dependent on river input, concentration of suspended sediments, rate of atmospheric deposition, and the rates of deposition and resuspension relative to radioactive decay (Sommerfield et al., 1999).

The activities of ^{137}Cs and ^{7}Be were determined through gamma spectroscopy analysis of dried sediment (661 KeV peak for ^{137}Cs and 477.7 KeV peak for ^{7}Be). After water weight loss measurements for porosity, a known mass of ground sediment was placed in a 6-cm diameter petri dish, sealed, and counted for 24 hours on a Canberra low-energy gamma detector. The minimum detectable activity used for ^{137}Cs is 0.05 dpm g^{-1}. Carbon-14 dating of selected shells was conducted at the University of Arizona AMS lab. The lab provided both the conventional ^{14}C ages and a calibrated ^{14}C ages.

Excess ^{210}Pb activities were determined through gamma spectroscopy. Excess ^{210}Pb was calculated by subtracting supported ^{210}Pb from total ^{210}Pb. Supported ^{210}Pb is determined by averaging the intermediate daughter products (^{214}Pb ($t_{1/2}$ = 26.8 min; 295.2 KeV and 352 KeV

peaks) and ^{214}Bi ($t_{1/2}$ = 19.7 min; 609 KeV peak) between ^{222}Rn and ^{210}Pb. The products are assumed to be in secular equilibrium with ^{210}Pb.

Vibracores collected in May 2003 were analyzed for excess ^{210}Pb through decay counting of ^{210}Po, assuming secular equilibrium between ^{210}Pb and its granddaughter ^{210}Po. Samples of 3-5 g were dried to determine porosity and then spiked with a known amount of ^{209}Po. The samples were dried to near dryness twice, first in the presence of HNO_3 and then in the presence of HCL in order to destroy organic matter and leach the ^{209}Po off of the sediments. Diluted HCL was added to the sample to create a solution of the residue. This solution was centrifuged to remove the particulates from the solution. Then isotopes ^{209}Po and ^{210}Po were removed from the solution through spontaneous electrodeposition onto silver planchets, and analyzed using a Canberra Alpha Analyst detector system (Nittrouer et. al., 1979; Noller, 2000).

Using steady-state solutions to the advective-diffusion equation and assuming a log-linear relationship between activity and depth, excess ^{210}Pb was used to determine sediment accumulation rates (S, cm/yr). Sediment accumulation rates were calculated for $^{210}Pb_{xs}$ profiles below the estimated bioturbation depth through the least-squares fit to the equation:

$$A_z = A_0 \exp(-\lambda z/s) \qquad (1)$$

where, S (cm/yr) = accumulation rate, λ (1/t) is the decay constant (0.693 / $t_{1/2}$), z is the depth in the seabed (cm), A_o is the excess activity at the surface (dpm/g) and A_z is the excess activity at depth z (dpm/g) (Goldberg, 1963; Koide et al., 1972; Appleby and Goldfield, 1979; Nittrouer and Sternberg, 1981).

Accumulation rates can also be estimated through ^{137}Cs the sediments using the equation:

$$(z - z_b) / \Delta t \qquad (2)$$

where z = the penetration depth of ^{137}Cs, z_b = the bioturbation depth or depth of mixing, and Δt = the elapsed time between the date of collection and 1954 (the date that ^{137}Cs was first released into the atmosphere). The depth of peak activity may also be used as a time marker of 1963 (when the release of ^{137}Cs into the atmosphere was at its peak) (Nittrouer and Sternberg, 1981; Sommerfield and Nittrouer, 1999).

Real-time Wave Data

Data from WAVCIS station CSI-13 (located at 89° 00’46’’N, 30° 15’967’’W in ~7 m of water) and the National Data Buoy Centers NDBC 42007 (located 40 km South-Southeast of Biloxi, MS at 30°05'24"N 88°46'12"W in ~13.5 m of water) (Fig. 2, Table 1) were collected during the period that Tropical Isidore and Hurricane Lili impacted the Northern Gulf of Mexico. Data collected from these two stations included: water level, significant wave height H_s, and wave period T_s. Wave friction velocities (***U_****) created by these two storms were calculated from the equations:

$$U_* = (2/3 * \pi)\, \rho\, f_w\, \tilde{u}_{bmax}^{\,2} \qquad (3)$$

where f_w is the wave friction factor defined as:

$$f_w = 2(u_{*w} / \tilde{u}_{bmax}^{\,2})^2 \qquad (4)$$

and $\tilde{u}_{bmax}$ is the maximum orbital velocity defined as:

$$|\tilde{u}_{bmax}| = a_b\, \omega \qquad (5)$$

in which a_b is the orbital semi-excursion (Wright, 1995).

Results

Box Cores

Box cores (Figs. 2-7, Table 1) display low bulk-density sediments as dark regions, and higher bulk-density sediments as bright regions in the X-radiographs. A variable sedimentary fabric that ranges from stratified (top 5-10 cm) to intensely bioturbated is visible in the x-radiographs from BC1, BC3, BC6, and BC12 (Figs. 3, 4, 5, and 6). Boxcores BC 3 and 12 contain layers of higher density, which corresponds to an increase in sand/silt concentration (Figs. 4 and 6). The higher density sandy layer in BC 12, occurring at depths 22-25 cm, has an erosional base and overlies muddy sediment, and a second high-density layer is visible in the X-radiograph at a depths 30-33 cm. The X-radiograph of BC 14 (Fig. 7) displays an upper low-density zone, extending to 11 cm below sea floor (bsf), overlying a more dense region of higher sand content.

Sediment accumulation rates were calculated through gamma spectroscopy of ^{210}Pb and ^{137}Cs. Profiles of ^{210}Pb in BC1 and BC6 display near constant activity throughout the core (Figs. 3 and 5). The upper 12-14 cm in both BC3 and BC12 display nearly constant activity (Figs. 4 and 6). Box cores BC3 and BC12 display depth-dependent profiles below surficial zones of constant activity. Apparent sediment accumulation rates were calculated using Equation 1 for BC3 and BC12. An accumulation rate for BC3 was calculated to be 0.45 cm yr^{-1} over the depth range 18 to 36 cm. BC12 displays two different depth-dependent profiles below the zone of constant accumulation. The apparent accumulation rate for the upper zone (14–24 cm in depth) was calculated to be 1.36 cm yr^{-1}. While the accumulation rate for the second zone (26-36 cm in depth) was calculated to be 0.71 cm yr^{-1}. In each core, ^{137}Cs was detected to base of each of the

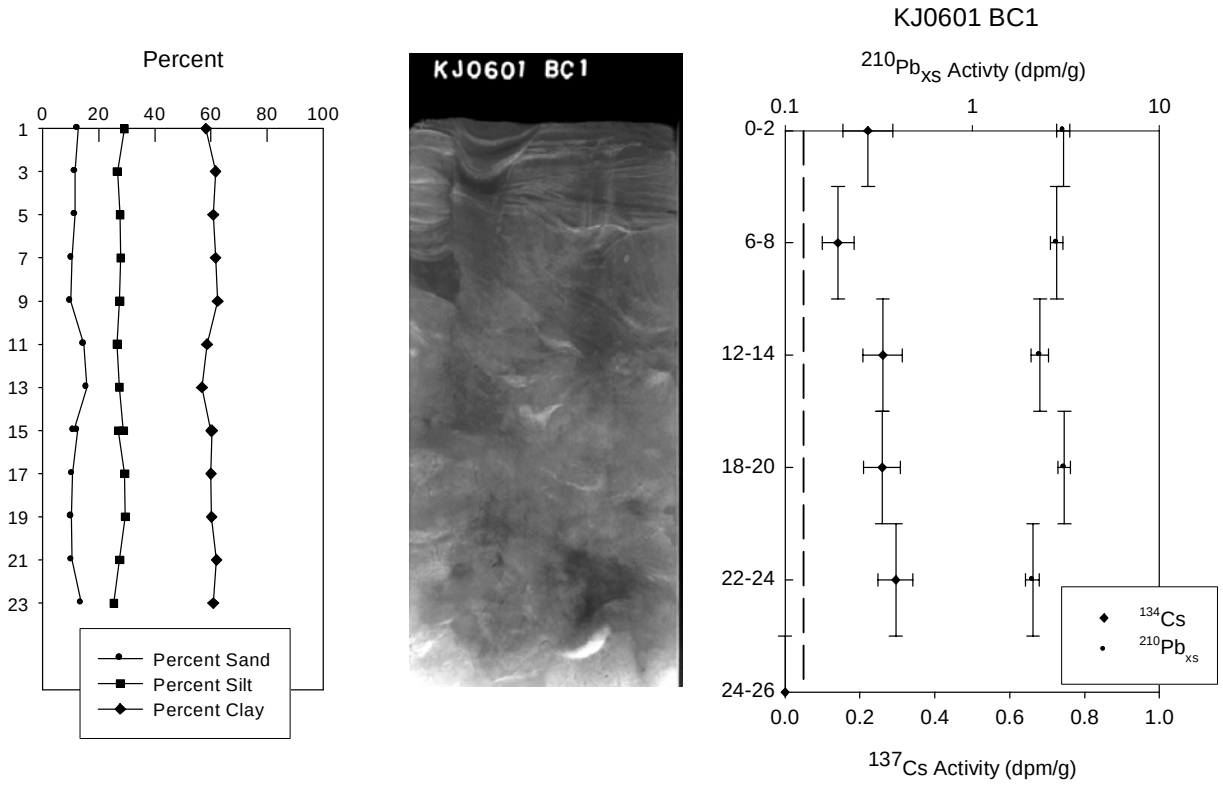

Figure 3. KJ0601 BC1 grain size, x-radiograph, and radiochemistry. ^{137}Cs penetrates the entire core.

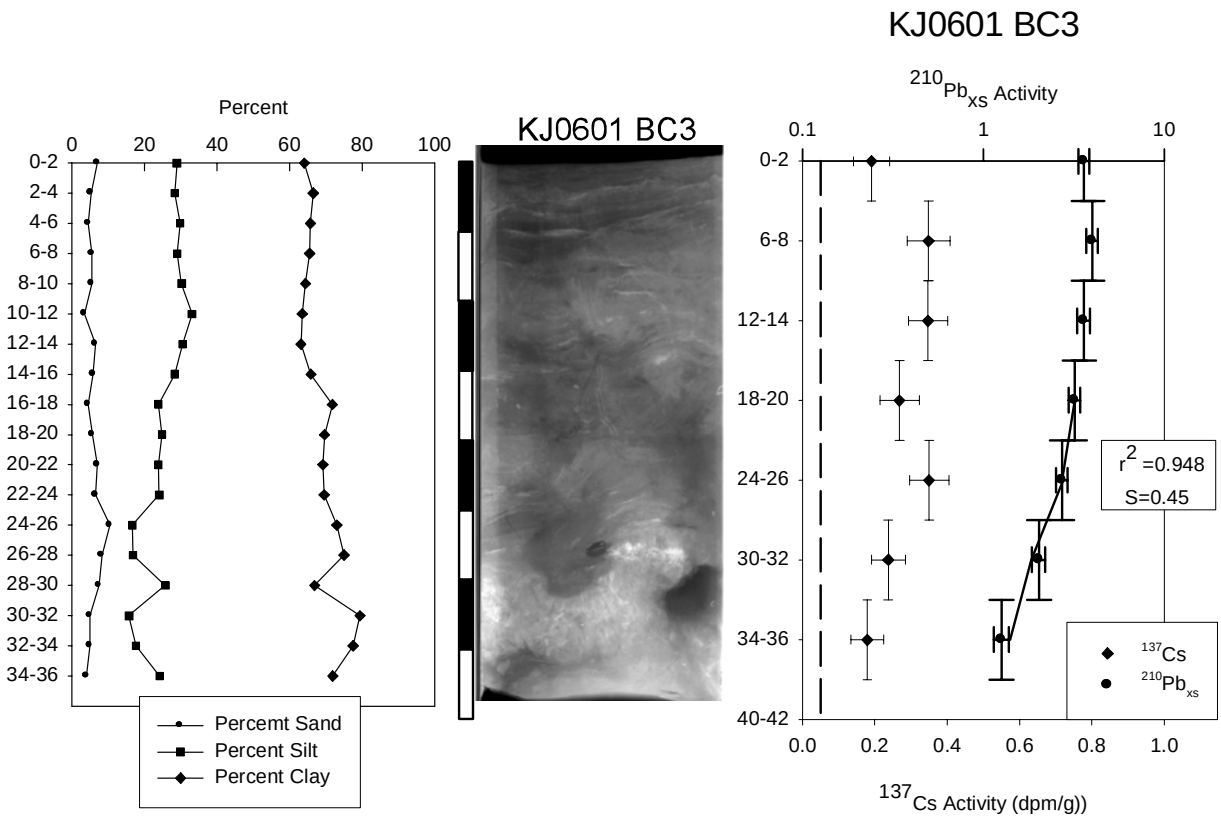

Figure 4. KJ0601 BC3 grain size, x-radiograph, and radiochemistry. ^{137}Cs penetrates the entire core.

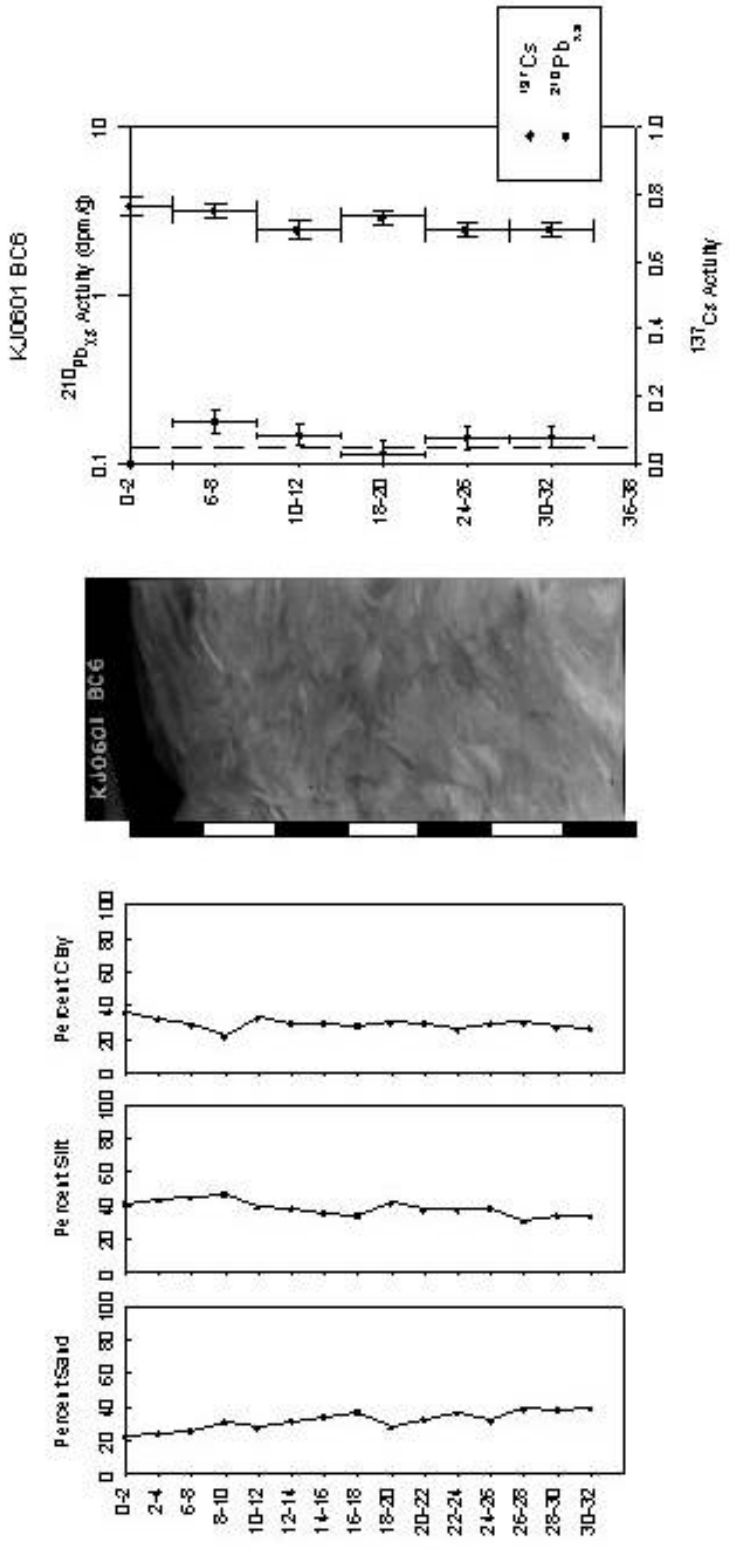

Figure 5. KJ0601 BC6. Grain size, x-radiograph, and radiochemistry. ^{137}Cs penetrates to 30 cm depth.

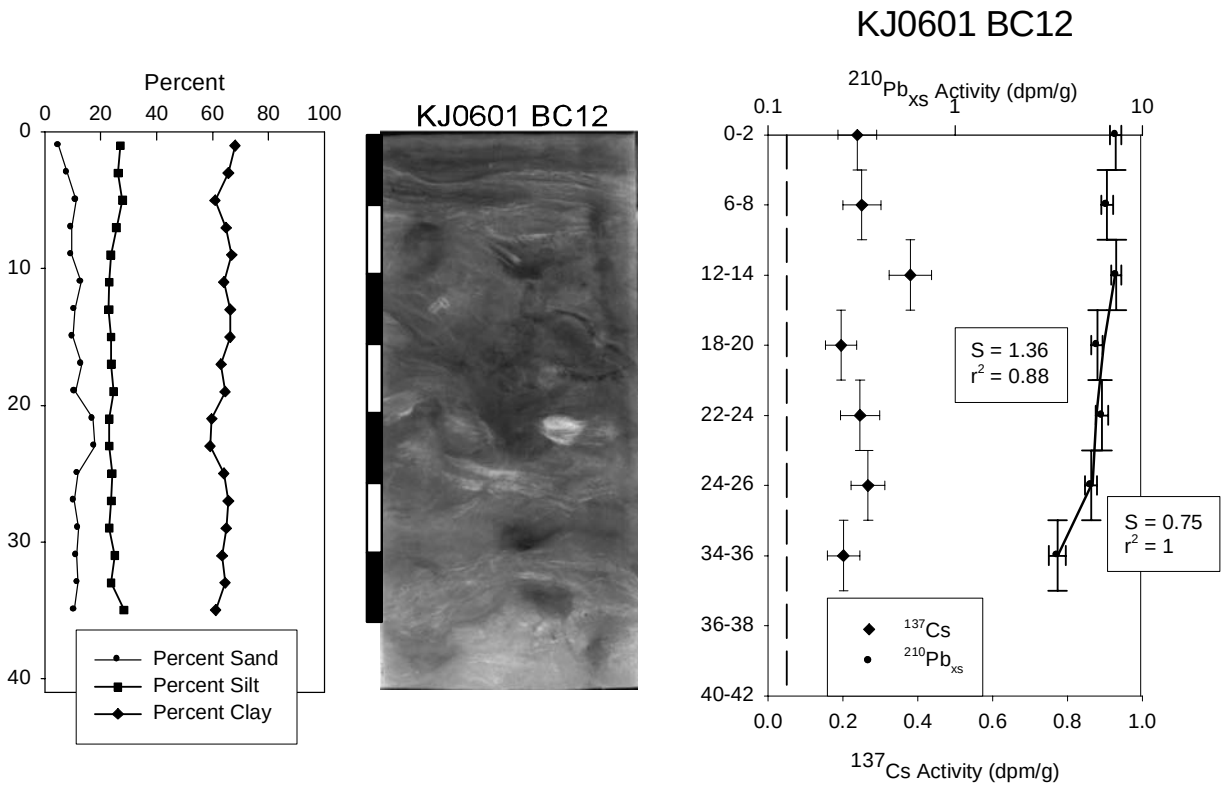

Figure 6. KJ0601 BC12 Grain size, x-radiograph, and radiochemistry. ^{137}Cs penetrates to ~35 cm depth.

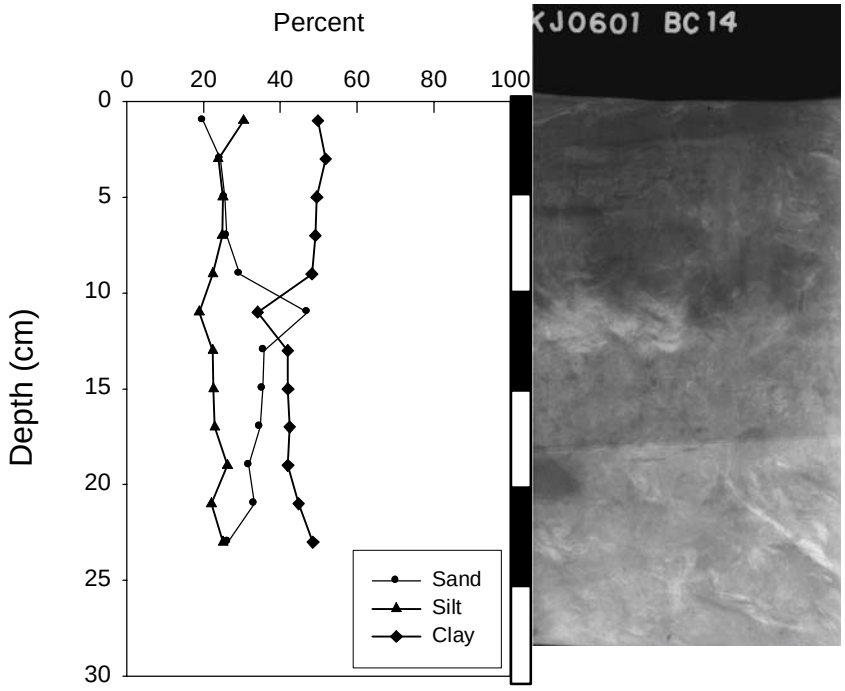

Figure 7. KJ0601 BC14 Grain size and x-radiograph

box cores; therefore only a minimum accumulation rate could be calculated. Minimum accumulation rates for the box cores ranged from 0.42 cm yr^{-1} in BC1 to 0.55 cm yr^{-1} for BC3 (Figs. 3 and 4), and are not inconsistent with ^{210}Pb apparent accumulation rates.

Gravity Cores and Vibracores

The X-radiographs of GC10 (Fig. 2, Table 1) displays surficial high porosity muds overlying stratified mud and sand, interbedded with bioturbated intervals of sandy mud (Fig. 8). Profiles of wet bulk density are characterized by a series of density maxima (such as ~15 and ~95 cm bsf) separated by regions of low density (1.5–1.65 g/cc). Three prominent spikes in the bulk density have maxima at or above 1.7 g/cc (spikes 1, 4, and 5; Fig. 8). A close-up of the X-radiograph displays that peak 5 is associated with a layer of shell hash (Fig. 8-D). Four peaks in the bulk density profile have maxima at approximately 1.65 g/cc (Spikes 2, 3, 6, and 7; Fig. 8). The X-radiographs reveal that these maxima are associated with sandy regions in the core. However, there are sandy regions displayed in the X-radiographs that do not correspond to density maxima in the bulk density profile (sand layers B and C; Fig. 8).

Excess ^{210}Pb profiles from GC10 display relatively constant activity in the upper 5-10 cm (Fig. 9). Below this interval, the profile displays a depth-dependent gradient. The constant activity in the top 5-10 cm is attributed to bioturbation and physical sediment mixing. Below this zone, the gradient is interpreted to be controlled by radioactive decay and sediment burial (Eq. 1). The apparent sediment accumulation rate calculated from Eq. 1 is 0.5 cm yr^{-1} over the depth interval 18 to 34 cm. Cesium-137 penetrated to a depth of 25 cm in GC10 (Fig. 9). Assuming a bioturbation depth of ~10 cm, this ^{137}Cs penetration translates to an accumulation rate of 0.31 cm yr^{-1} since 1954, somewhat lower than the ^{210}Pb rate, which integrates sedimentation rates over ~100 yr, or five half-lives of ^{210}Pb. For radiocarbon analysis, bivalves were identified through

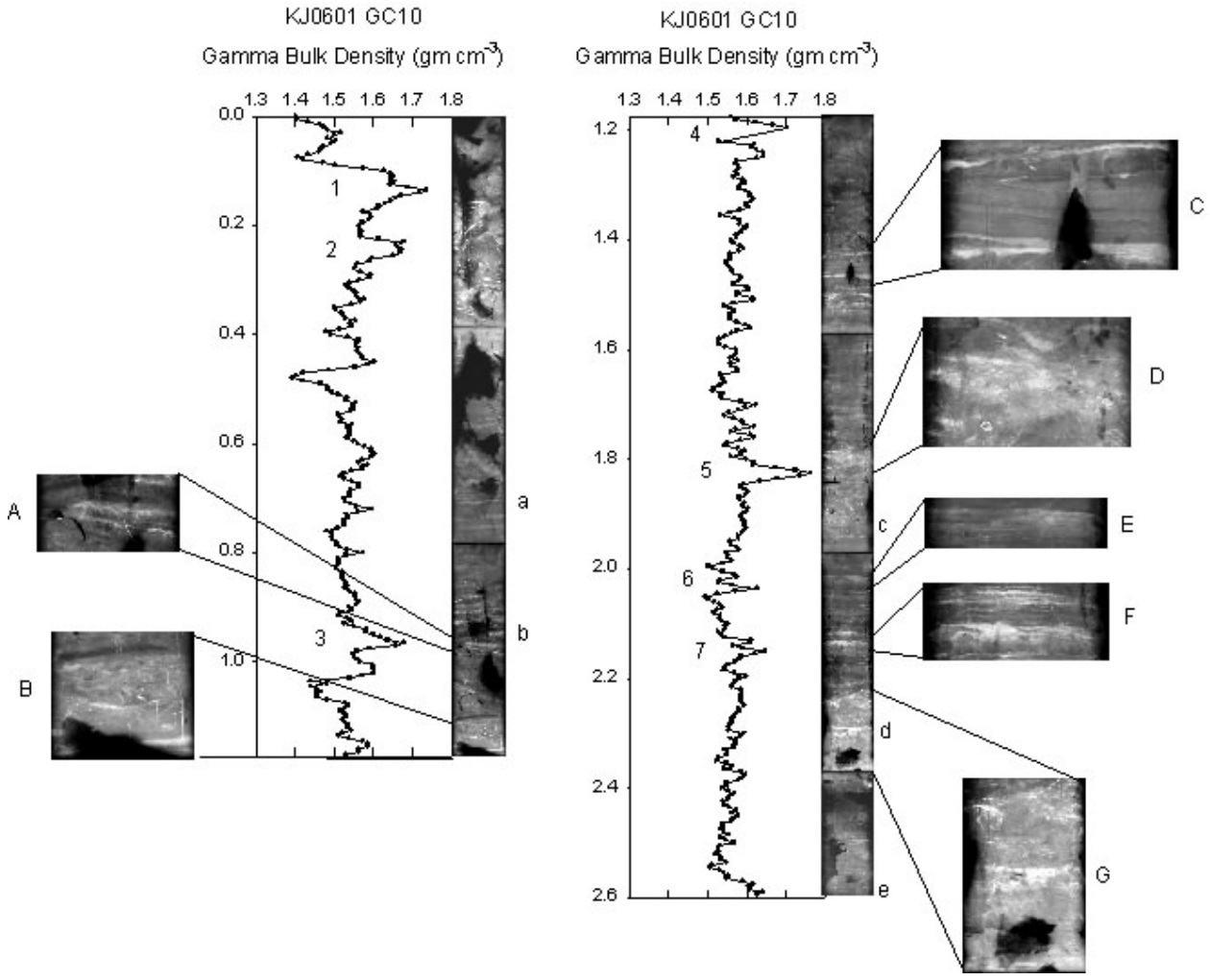

Figure 8. X-radiograph and gamma bulk density of KJ0601 GC10. Details of sand layers in x-radiographs are displayed in A, B, C, D, E, F, and G. Locations of shells for ^{14}C dating listed in table 2 are located at a, b, c, d, and e.

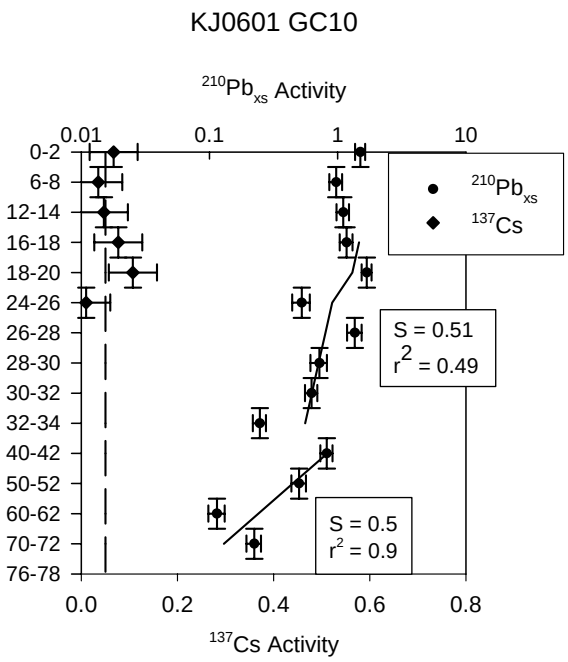

Figure 9. ^{210}Pb and ^{137}Cs of KJ0601 GC10

the X-radiographs of GC10 at selected intervals (Fig. 8). These were then analyzed for radiocarbon through accelerated mass spectrometry at the University of Arizona AMS laboratory. Corrected and calibrated, ages were used to calculate accumulation rates of ~0.3 cm yr^{-1} over the depth range of 0 to 2.61 m (Table 2).

Vibracore VC 2 (Fig. 2, Table 1) is located north of the recently formed spit of Horn Island and on the eastern fringe of the shipping channel between Horn Island and Ship Island. The top 0.8 m is dominated by shell hash in a sandy-mud matrix (Figs. 10 and 11). The X-radiographs and grain size data display a zone between 0.8 m and 1 m where the core becomes sandier with less shell hash present (Figs. 10 and 11). The gamma bulk density is near constant at ~1.75 g cm^{-3} throughout the core, except for a section between 0.3 and and 0.6 m depth that has a higher bulk density near 2.1 g cm^{-3} and sand content >80%. The gamma bulk-density profile for the bottom 0.5 m of the core displays a nearly constant bulk-density of ~1.7 g cm^{-3} with local maxima that correspond to features in the x-radiograph (Fig. 10). Grain size data for this interval displays a sand content of ~ 55% and mud content of ~ 45%.

Vibracore TM0503 VC15, located north of Petit Bois Island (Fig. 2, Table 1), displays a gradual increase in bulk density in the upper 1 m of the core (Fig. 12). The x-radiographs are characterized by low-density muddy sediment, represented by darker regions, to a depth of ~1m (Fig. 13). The x-radiographs become brighter with fewer regions of lower bulk density below 1-meter depth. The images display a more mottled sedimentary fabric with depth until about 1.7 m bsf. Below this depth, there is a lack of sedimentary structure displayed X-radiographs and a higher, near constant bulk-density. A sharp contact occurs at ~2.45 m where the sediment changes from a gray muddy sand to compacted bluish-green silty-clay.

Table 2. ^{14}C dates from KJ0601 GC10.

Sample #	Date Collected	Sample Material	Depth In Core (cm)	Comments	13Cδ	Corrected 14C age (BP)	Calibrated age range (2s)
a	Jun-01	Shell	67.5		-6.83	2185 +- 71	397 - 5 BC
b	Jun-01	Shell	87.5	lost by UA-AMS	---	---	---
c	Jun-01	Shell	185		-2.55	2091 +- 52	349 - 45 BC
d	Jun-01	Shell	228		-4.88	2185 +- 65	395 - 47 BC
e	Jun-01	Shell	261		-3.49	2340 +- 67	758 - 207 BC

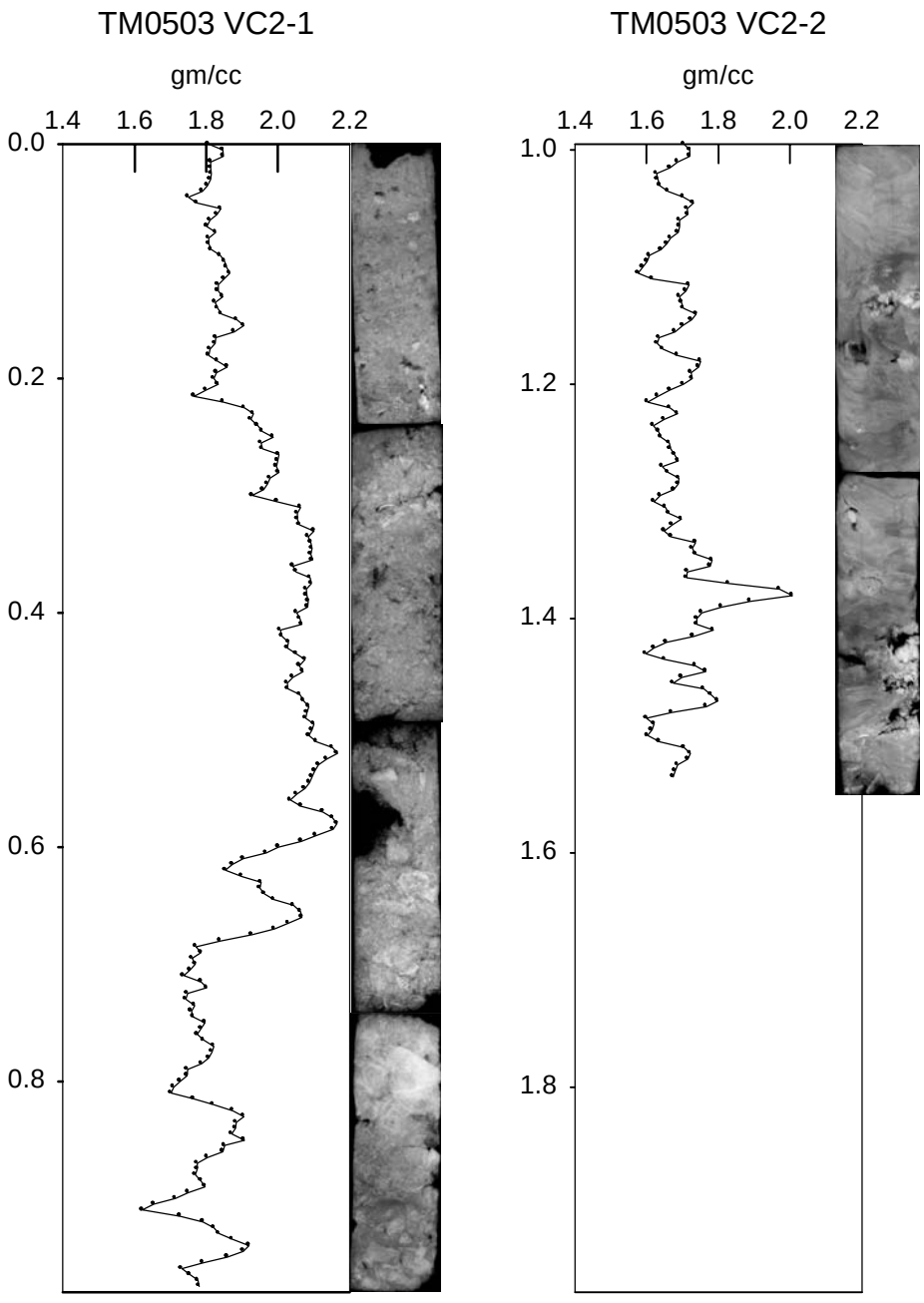

Figure 10. Gamma bulk density and x-radiograph of TM0503 VC2

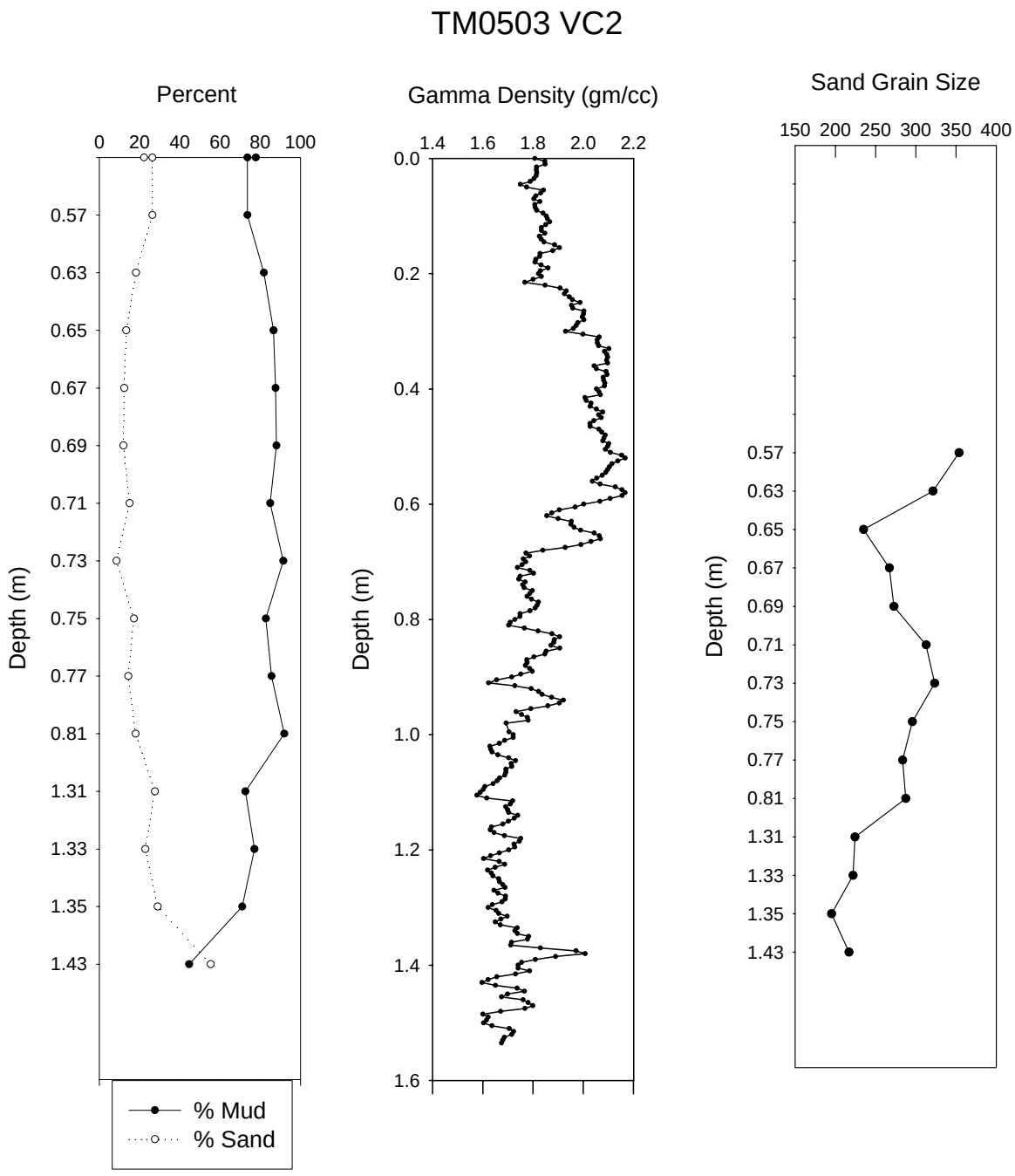

Figure 11. Grain size data and gamma bulk density for TM0503 VC2

TM0503 VC15

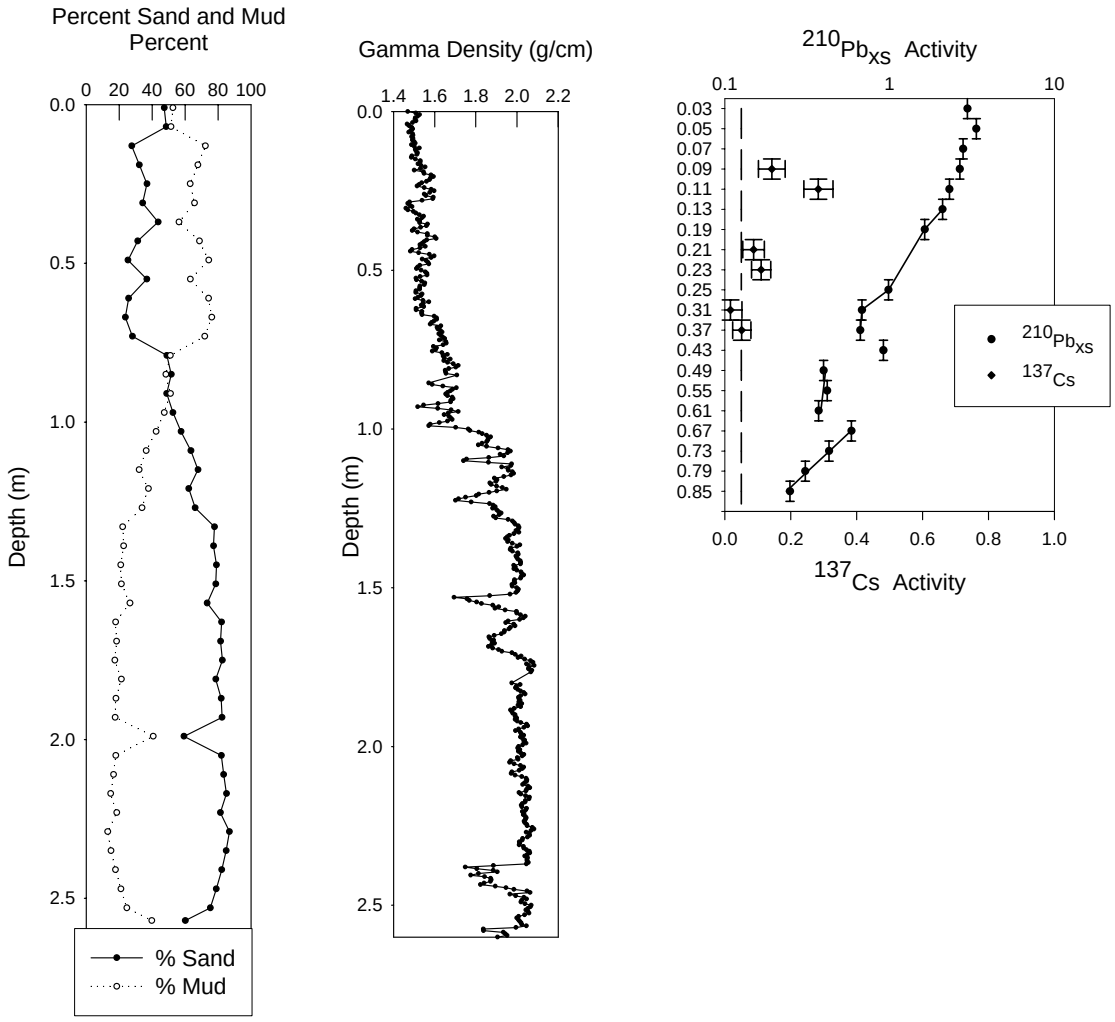

Figure 12. Grain size, gamma bulk density, and radiochemistry data for TM0503 VC15.

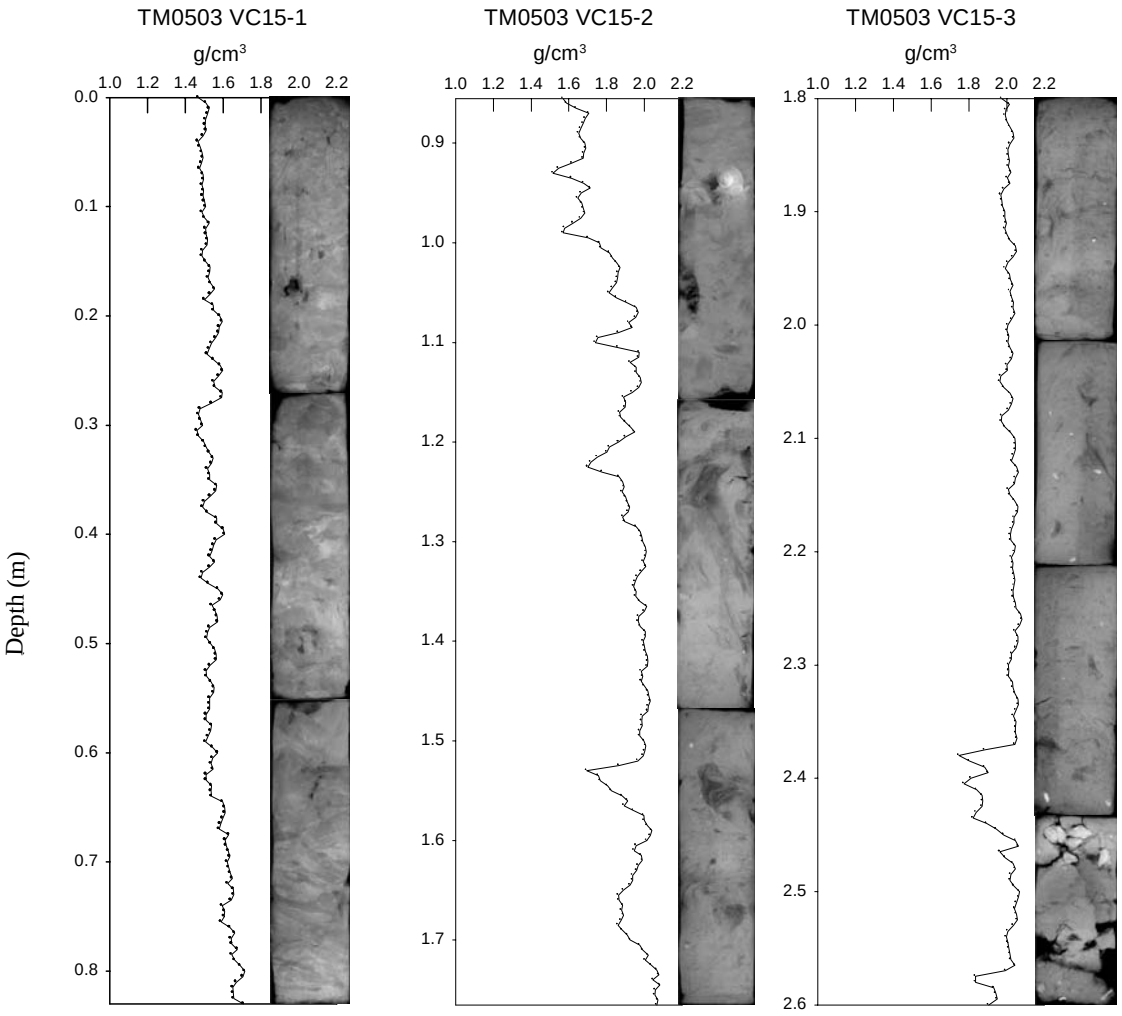

Figure 13. X-radiographs and gamma bulk density of TM0503 VC15

Granulometric data (Fig. 12) display sandy-mud overlying muddy-sand, with a downward increase in the sand content beginning at 78-80 cm bsf. Sand content continues to increase to a depth of ~1.3m, below which the sand content is roughly constant. This depth range corresponds to the region of constant bulk density. The coarse sediment fraction from 0.92 to 2.24 m depth was analyzed using a settling column. The results showed a mean grain size of 250 μm ± 10.

Profiles of excess ^{210}Pb activities display a zone of near constant activity in the top 8-10 cm (Fig. 12). Below this depth, the profile displays a depth-dependent profile with exponentially decreasing activity between 12-24 cm bsf and 68-86 cm bsf. A ragged, stair-step zone of activity between 30 and 6 cm bsf likely resulted from some buried disturbance zone or bioturbation zone. Accumulation rates, calculated by plotting a regression of the two depth-dependent slopes, are 0.49 cm yr^{-1} between 12 cm and 24 cm and 0.61 cm yr^{-1} between 68 cm and 86 cm (Fig. 12). An unambiguous peak in ^{137}Cs activity is not present; however, ^{137}Cs had a maximum penetration depth of 22 cm ± 2 cm, yielding an accumulation rate of 0.32 cm yr^{-1}.

The X-radiographs of VC17 (Fig. 2, Table 1) display a zone of homogenized sediment in the top 0.5 m of the core (Fig. 14). Grain size data display a downward decreasing clay content and increasing sand content within this interval (Fig. 15). The X-radiographs display an increased occurrence of higher density sediment, displayed as brighter images, below this interval. These higher density intervals correspond to increases in the sand content in the grain size data (Figs. 14 and 15). Bulk density data display a gradual increase in gamma bulk density (~1.2 to 1.5 g cm^{-3}) with increasing depth in the top 1.15 m of the core, which corresponds to increasing sand content with depth in the grain size data. Peaks of maxima gamma bulk density correspond to sandy layers displayed in the X-radiographs (Fig. 14 B and C). A sharp contact at

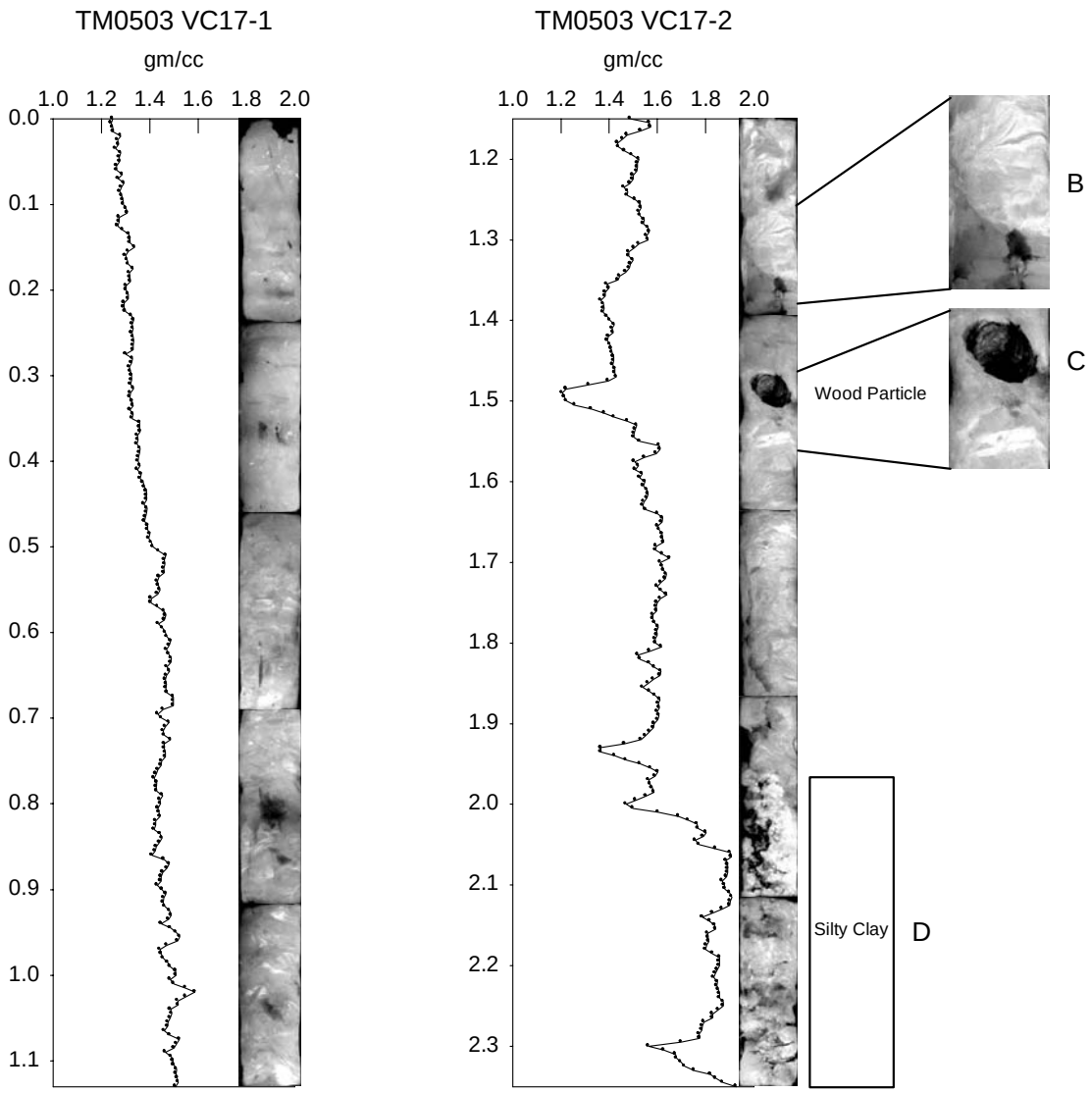

Figure 14. X-radiographs and gamma bulk density of TM0503 VC17.

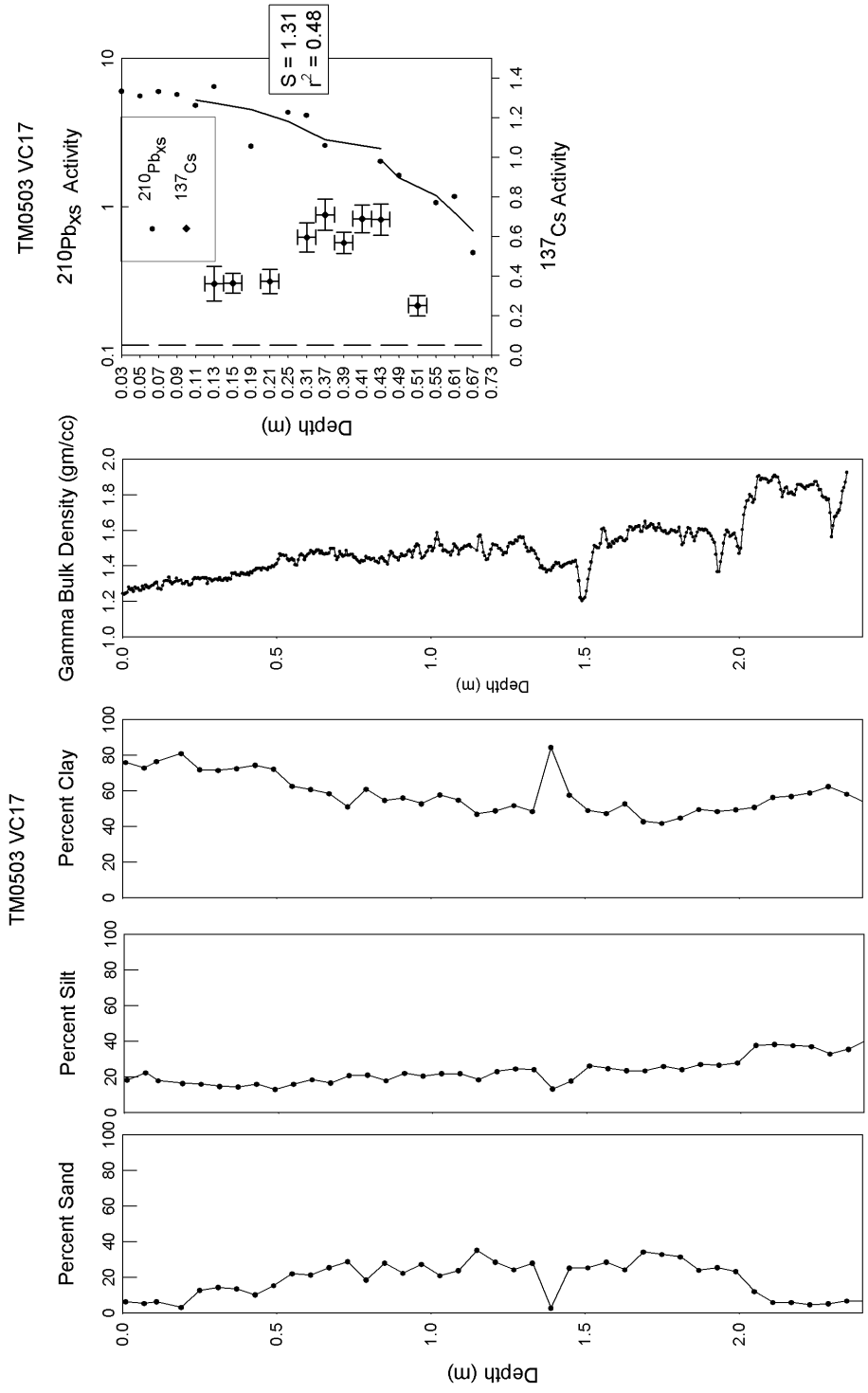

Figure 15. Grain size, gamma bulk density, and radiochemistry for TM0503 VC17.

~2 m marks a change in sediment type from gray muddy sand to compacted bluish-gray silty-clay, which persists to the bottom of the core (Fig. 14-D).

Profiles of excess ^{210}Pb activities display a zone of near constant activity in the top 8-10 cm (Fig. 15). Below this depth, the profile displays a depth-dependent profile with decreasing activity, and an obvious change in sedimentation rate around 42 cm bsf (circa 1970). Accumulation rates, calculated by plotting a regression of the two depth-dependent slopes, are 1.31 cm yr^{-1} (between 12-40 cm) and 0.67 cm yr^{-1} (between 44-68 cm) (Fig. 15). Maximum activities of ^{137}Cs occur between 38 and 44 cm (Fig. 15); however, an accumulation rate of 0.82 cm yr^{-1} was calculating by using the depth of ^{137}Cs penetration, 50 cm ± 2 cm.

Vibracore VC 18 (Fig. 2, Table 1) had a shallow penetration depth of 65 cm. An increase in bulk density at 18-20 cm denotes the top of a highly compacted sandy-clay that persists throughout the rest of the core (Fig. 16). Granulometric data (Fig. 16) show a slight increase in sand content in the upper 14 cm followed by a constant proportion of sand, silt, and clay throughout the rest of the core. A profile of excess ^{210}Pb (Fig. 16) displays a zone of near constant activity in the top 6 cm of the core, below which a depth-dependent gradient extends from 6 to 20 cm. Below ~20 cm the profile displays nearly constant activity of ~2 dpm g^{-1} over the 6-20 cm interval. A regression yielded an accumulation rate of 0.11 cm yr^{-1}. Activities of ^{137}Cs were below detection limits.

The average gamma bulk-density of VC16 is ~2.0 g cm^{-3} (Fig. 17). This value persists throughout the core. A visual inspection of the core showed a muddy silty-sand with abundant shell at the top of the core overlying more compacted sands. Clean sands dominate the base of the core. The mean grain size of the sand fraction of the core is between 220µm and 380µm (Fig. 17).

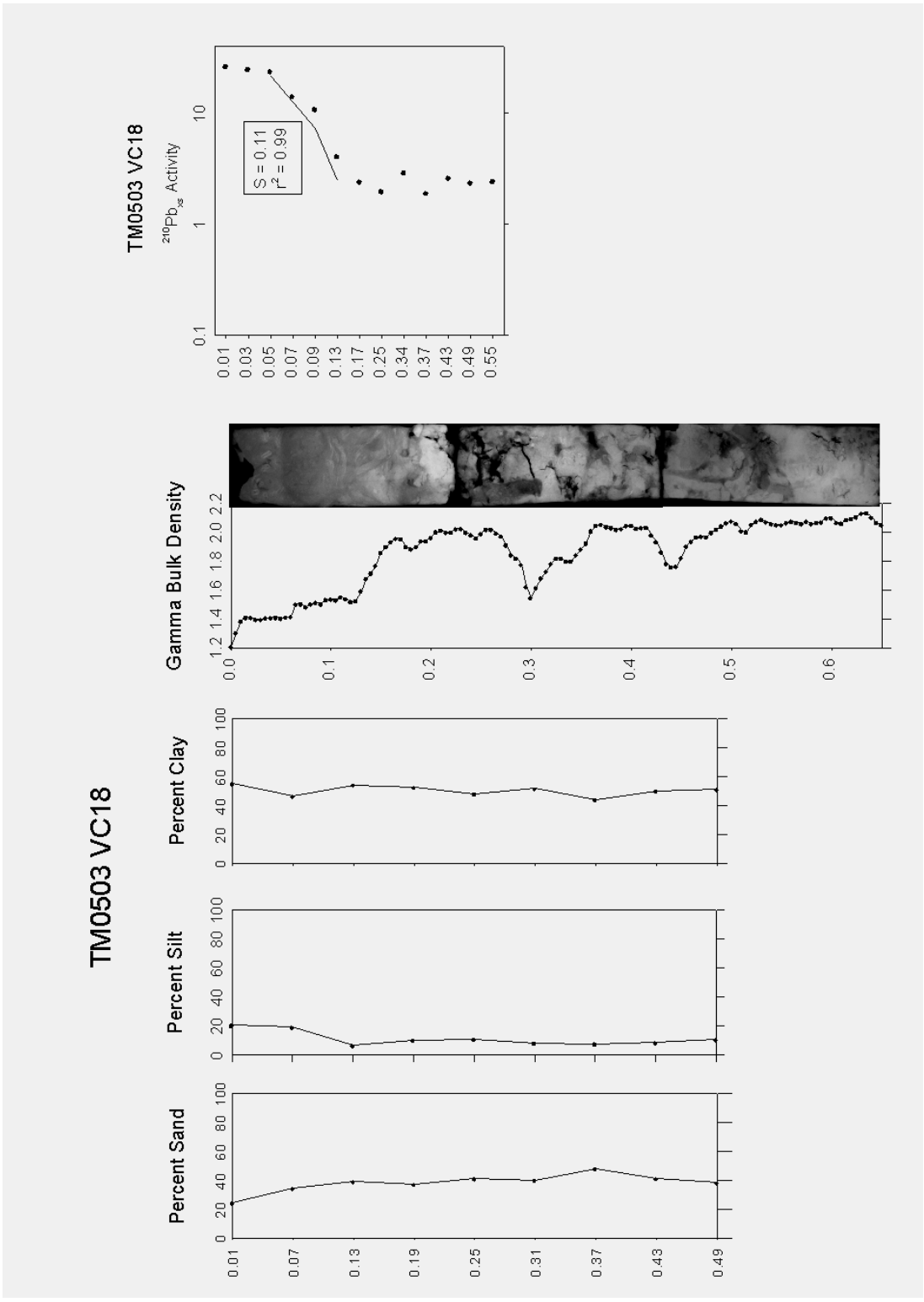

Figure 16. Grain size, gamma bulk density, x-radiography, and radiochemistry for TM0503 VC18.

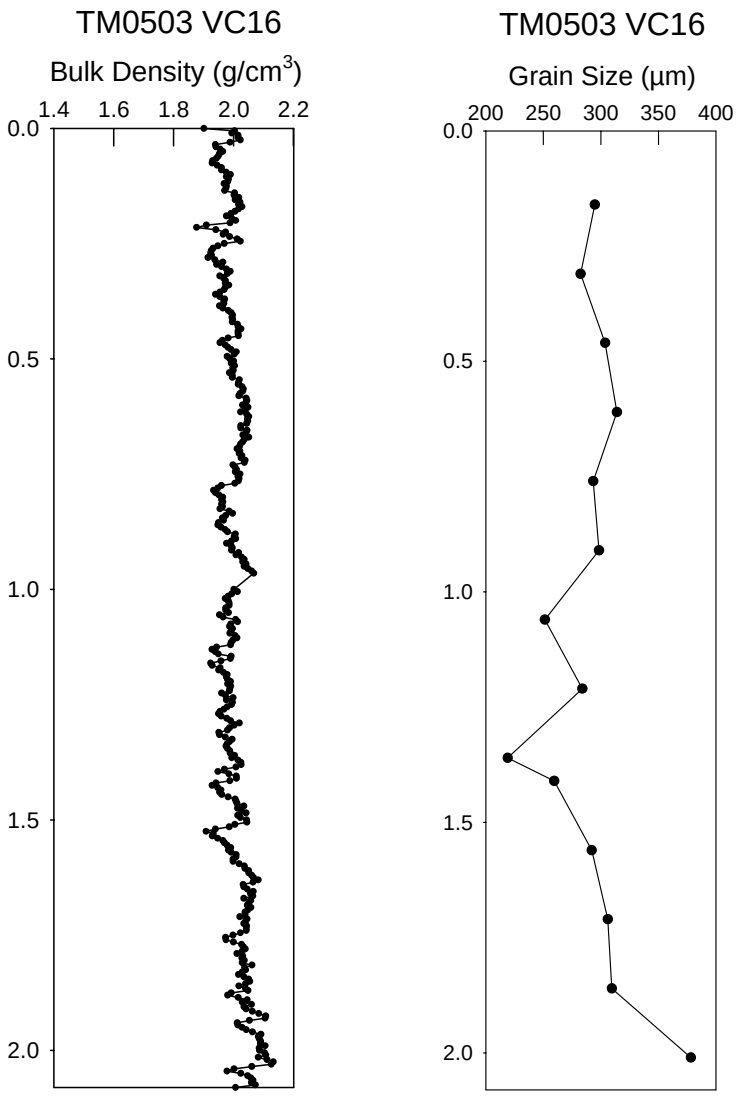

Figure 17. Gamma bulk density and mean grain size of the sand fraction of TM0503 VC16.

Transects

Cross section A-A' (Fig. 2) is a north-south transect above the northern spit of Cat Island that encompasses vibracores VC28, VC27, and VC26 (Fig. 18). Correlations shown are based on gamma density data that vary chiefly due to variations in grain size. Vibracores VC28 and VC27 are composed of a muddy sediment facies overlying a sandy facies. However, VC26 displays a sand facies overlying a mud facies.

The gamma bulk-density profile for TM0503 VC28 (Fig. 19) displays a nearly constant density of ~1.4 g cm^{-3} over the depth range of 0-1.2 m bsf. Over the depth range 1.2-1.45 m bsf, density increases to 1.8 g cm^{-3}, and remains nearly constant to the base of the core. Grain size data (Fig. 19) reflects the changes in the bulk-density data throughout the core. The top 1.16 m of the core is greater than 90% mud; however, between 1.16 m and 1.4 m the concentration of sand increases. The core becomes greater than 50% sand at ~1.45 m and remains sandy throughout the rest of the core. The X-radiographs of VC28 (Fig. 20) display a bioturbated sedimentary fabric with few lenses of sand until ~1.22 m bsf. At this point the radiographs display sandy layers and lenses.

Grain size data for TM0503 VC26 (Fig. 21) displays sandy mud sediment in the top ~1.0 m of the core. At approximately 1.1 m the concentration of mud increases to > 90%. The gamma-bulk density profile reflects this change in sediment type as the profile becomes nearly constant at ~1.4 g cm^{-3}. The X-radiographs of VC26 (Fig. 22) display sandy layers as brighter layers in the images. These sandy layers correspond to density maxima in the bulk-density data. Below ~1.1 m depth, the X-radiographs display a decreased occurrence of sandy layers interbedded within a bioturbated muddy sedimentary fabric.

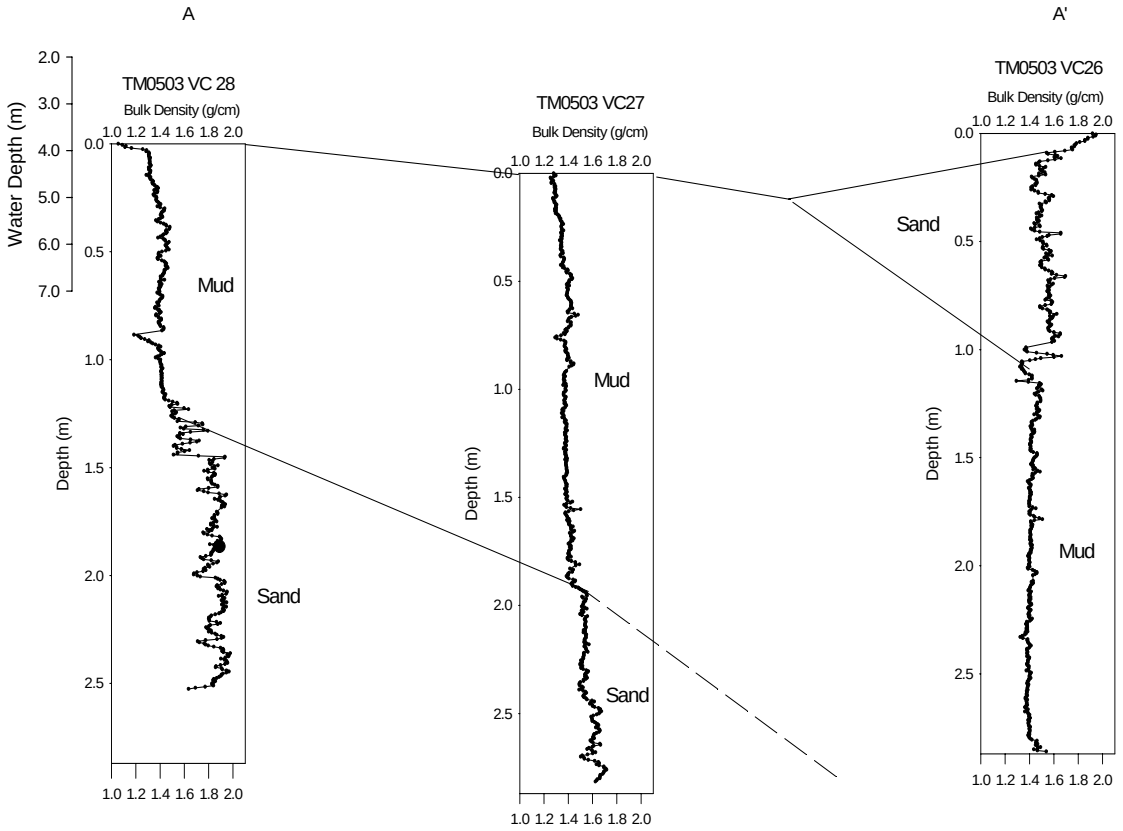

Figure 18. Cross section of A to A'. Gamma bulk density profiles of TM0503 VC28, VC27, and VC26.

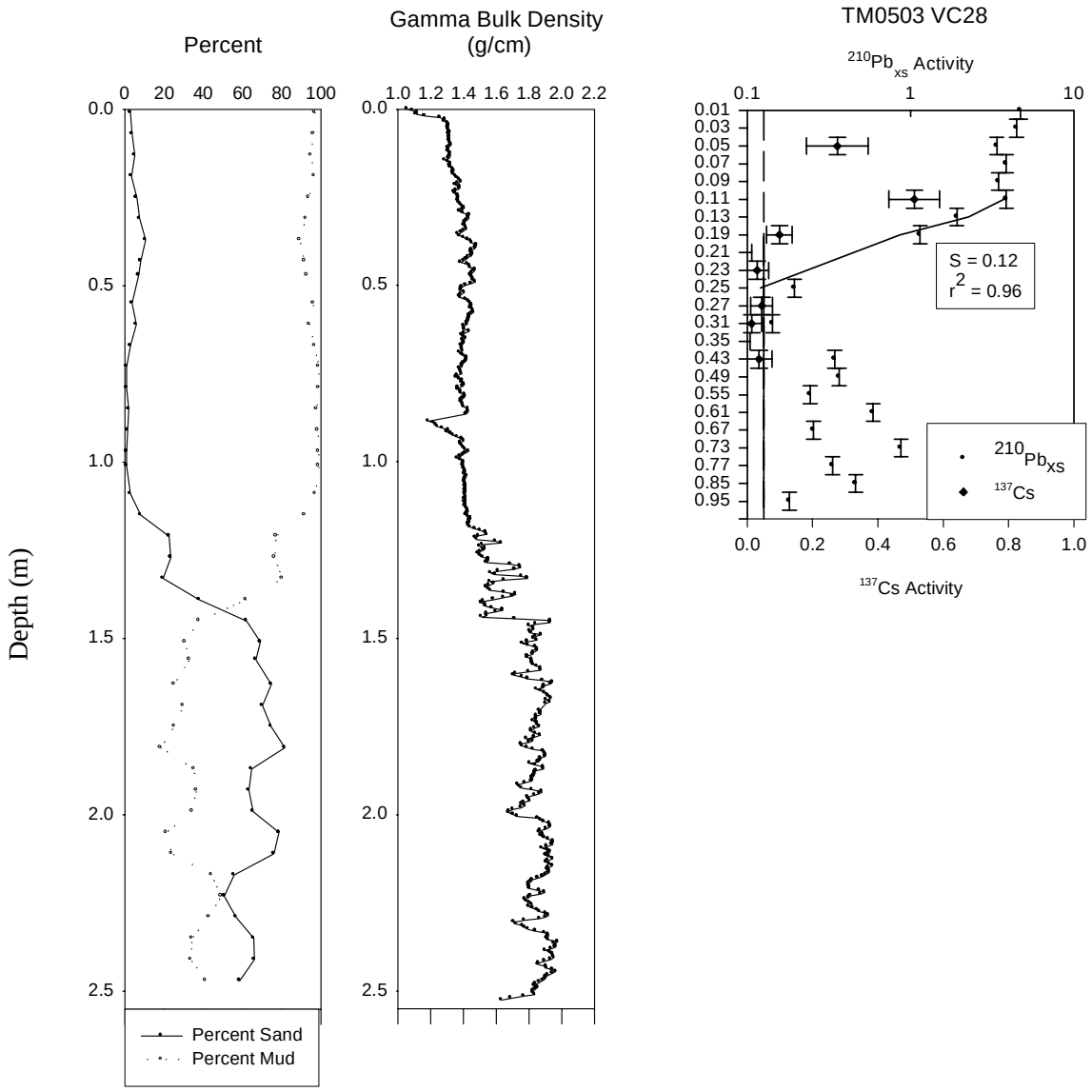

Figure 19. Grain size, gamma bulk density, and radiochemistry for TM0503 VC28.

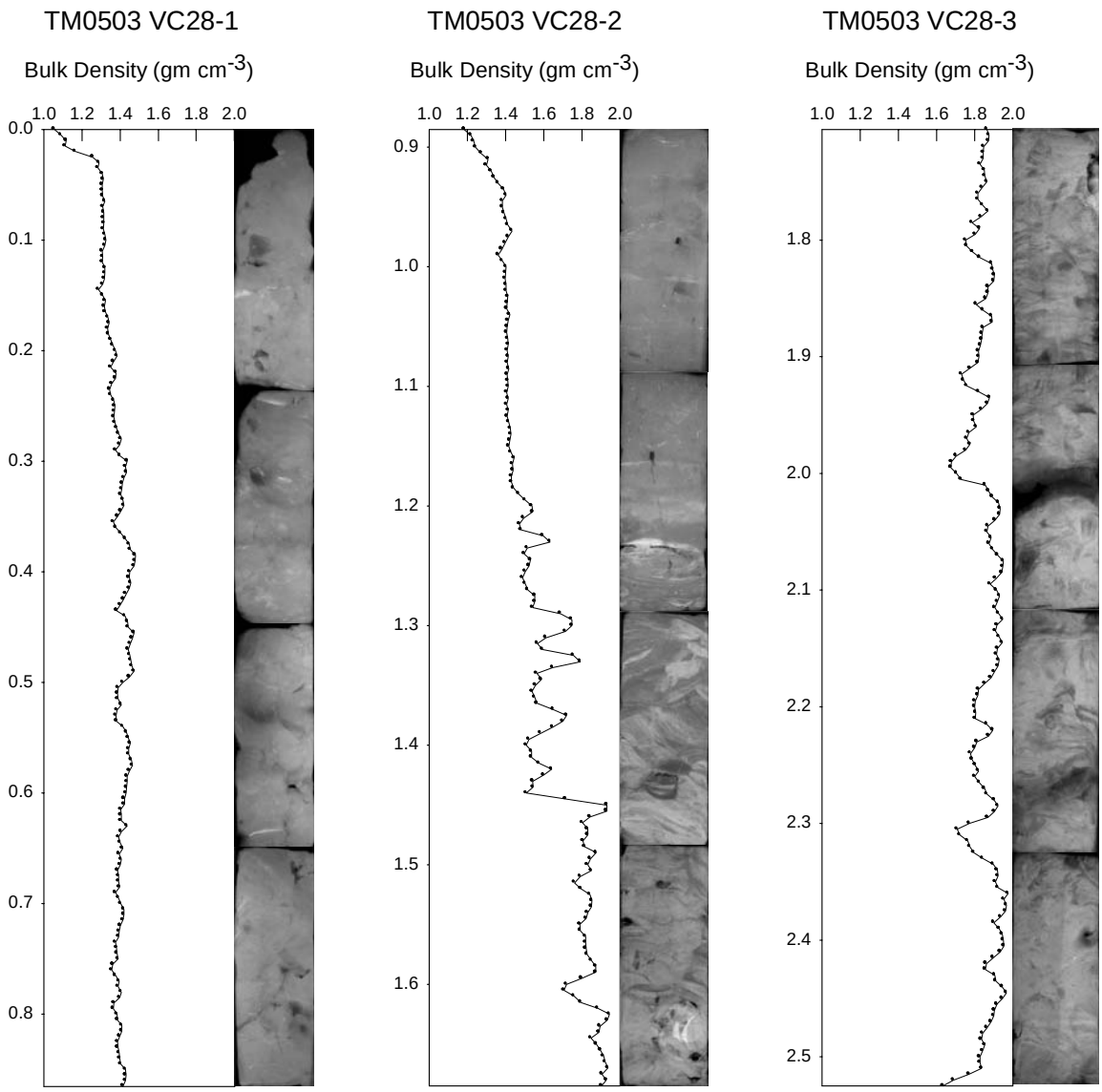

Figure 20. Gamma bulk density and x-radiographs for TM0503 VC28.

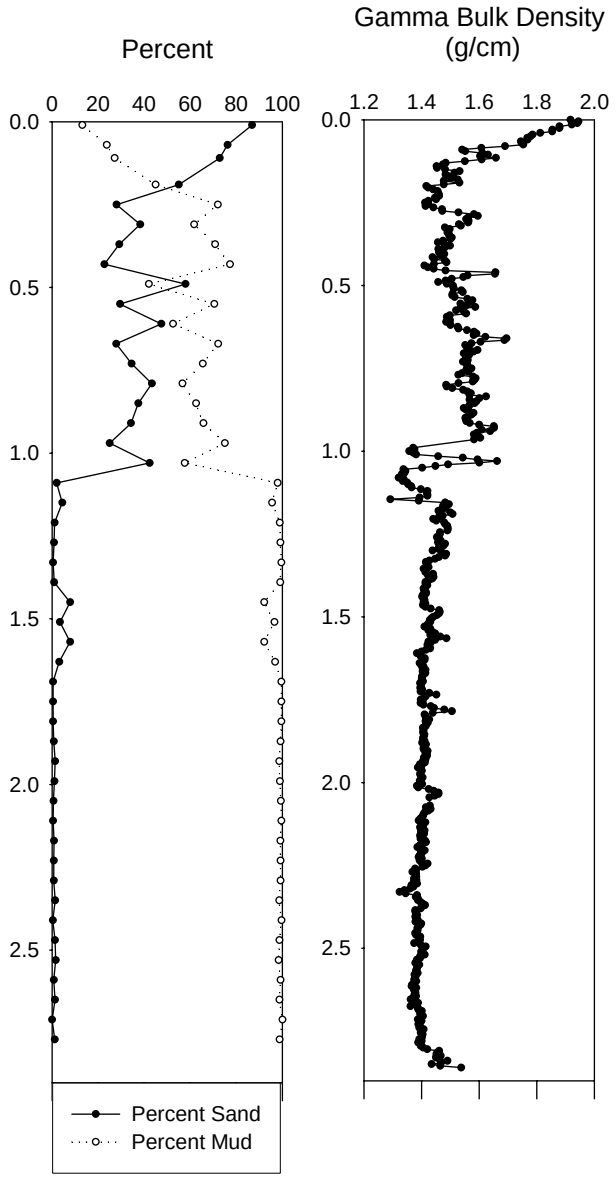

Figure 21. Grain size and gamma bulk density for TM0503 VC26.

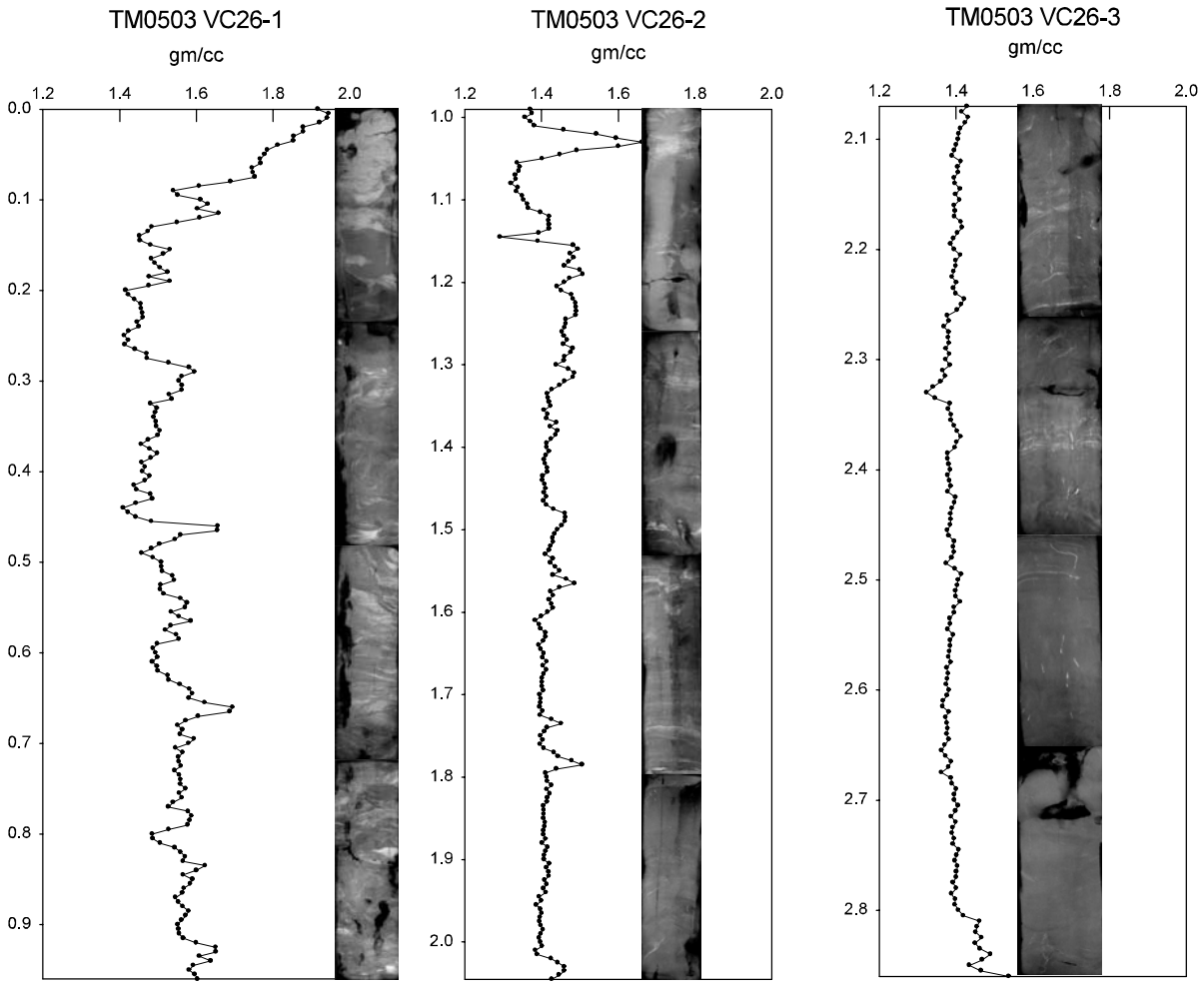

Figure 22. Gamma bulk density and x-radiographs for TM0503 VC26.

Excess ^{210}Pb activities for VC26 and VC28 (Fig. 19) were calculated through alpha spectroscopy and gamma spectroscopy of ^{137}Cs. Excess ^{210}Pb and ^{137}Cs activities were below detectable levels in VC26, which may be due to the high sand content in the upper ~1 m of the core. For VC28 the upper 10-12 cm displays near constant activity of excess ^{210}Pb. Below this depth, the profile displays an exponential decrease from 12 to 28 cm. Below 28 cm, the profile displays an increased activity; however, no trend can be identified. The calculated accumulation rate for the depth interval between 12 and 28 cm is 0.12 cm yr^{-1}. The penetration depth of ^{137}Cs is 20 cm ± 4 cm (Fig. 19) from which, an accumulation rate of 0.2 cm yr^{-1} was calculated.

Gamma bulk-density data of VC27 (Fig. 18) displays a nearly constant density of ~1.4 g cm^{-3} in the top 1.9 m. Below this depth the profile displays an increase in bulk density of greater than 1.5 g cm^{-3}, which persists to the bottom of the core. Vibracores VC26 and VC28 display an association between gamma bulk density and grain size. An increase in bulk density is associated with an increase in sand content in the cores (Figs. 19 and 21). Therefore, the gamma bulk density profile of VC27 suggests a muddy sediment facies overlying a sandy facies downcore.

Cross section B to B' (Fig. 2) is a north-south transect north of West Ship Island that encompasses vibracores VC14, VC13, and VC12 (Fig. 23). The gamma bulk density profile for VC14 displays near constant density of ~1.4 g cm^{-3} in the top 2.1 m bsf. Below this depth, the bulk density increases with depth to a depth of ~2.7 m bsf, at which the bulk density reaches a maximum of ~1.7 g cm^{-3}. The increase in bulk density in VC14 correlates to a similar increase in bulk density in VC13 between the depths ~1.5 to ~2.3 m bsf.

The top 1.4 m of VC13 displays a gamma bulk-density profile near ~1.4 with small peaks up to ~ 1.5 g cm^{-3} (Fig. 24). The ^{210}Pb profile displays activities of excess ^{210}Pb that are below detectable levels to a depth of 54 cm (Fig. 24). Below this depth the ^{210}Pb profile

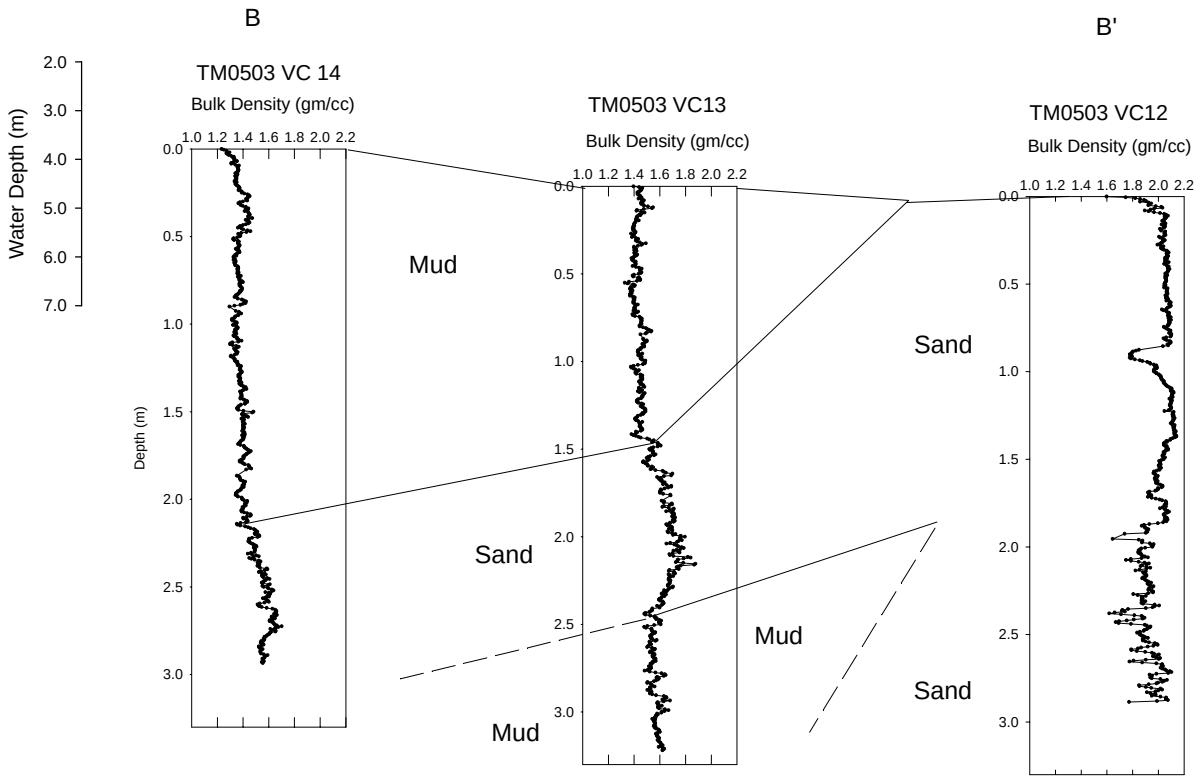

Figure 23. Cross section of B to B'. Gamma bulk density profiles of VC14, VC13, and VC12.

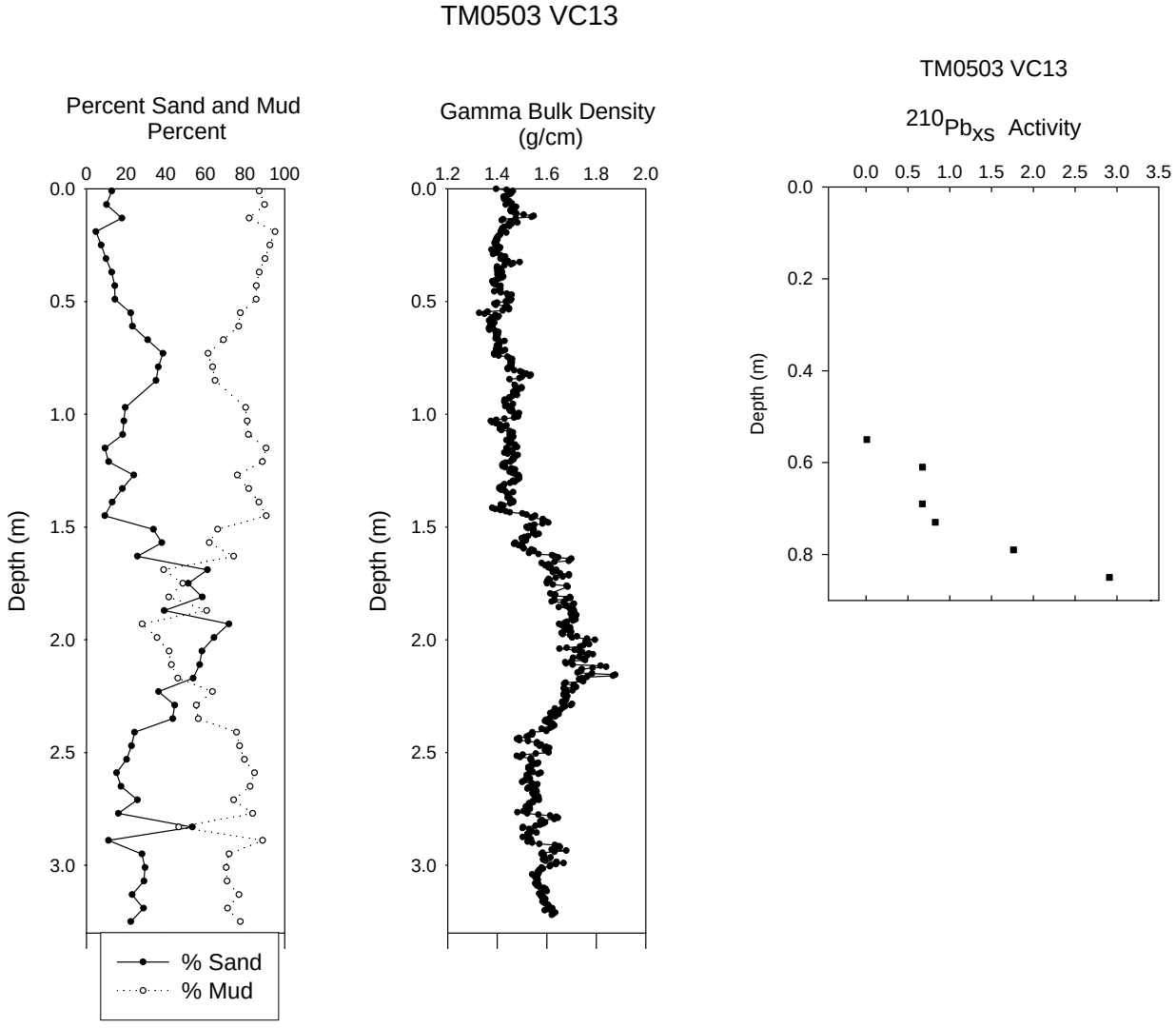

Figure 24. Grain size, gamma bulk density, and radiochemistry for TM0503 VC13.

displays a depth-dependent profile of increasing activity with depth. This is interpreted to be the result of dredge spoils being deposited in this location. Younger material was dredged and deposited first, followed by the subsequent deposition of older dredge spoil. X-radiographs display well-mixed sediment with no sedimentary structures of low density to a depth of ~1.2 m bsf, where an erosional contact is visible (Fig. 25-A). Below this contact, the x-radiographs display stratified muds and sands throughout the rest of the core.

The gamma density profile displays an increase in bulk density from 1.6 g cm^{-1} to >1.8 g cm^{-1} between the depths of ~1.5 m to ~2.15 m. The profile then displays a decrease in gamma bulk density (from >1.8 g cm^{-3} to ~1.5 g cm^{-3}) within the depth interval from 2.15m to 2.3 m (Fig. 24). The grain size data displays an increase in the sand content to greater than 70% followed by a decrease in content to less than 50% with the same depth intervals as the rise and fall in gamma bulk density (Fig. 24) Within the bottom 1.8 m of the core, X-radiographs display four basal sand layers. These layers are overlaid by laminated mud and sand, and three of the four layers (Figs. 25-C, D, and E) correspond to peaks in the gamma bulk density profile.

Vibracore VC12 (Fig. 23), located ~3.5 km south of VC13, is characterized by high gamma bulk density values throughout the core. The top ~1.8 m of the bulk density profile is near constant at 2.0 g cm^{-3}. Below this depth the core displays a more variable bulk density profile; however, the values are still above ~1.8 g cm^{-3}.

Cross section C to C' (Fig. 2) is an east-west transect encompassing cores VC14, VC25, and VC11 (Fig. 26). The three cores all display low gamma bulk density values in the tops of the cores. Vibracore VC14 displays low values (~1.4 g cm^{-3}) to a depth of 2.1 m. Below this depth, the bulk density increases with depth from ~1.5 g cm^{-3} to ~1.7 g cm^{-3}. Vibracore VC25, located ~9.5 km west of VC14, displays three trends in the gamma bulk density profile. The top ~0.7 m

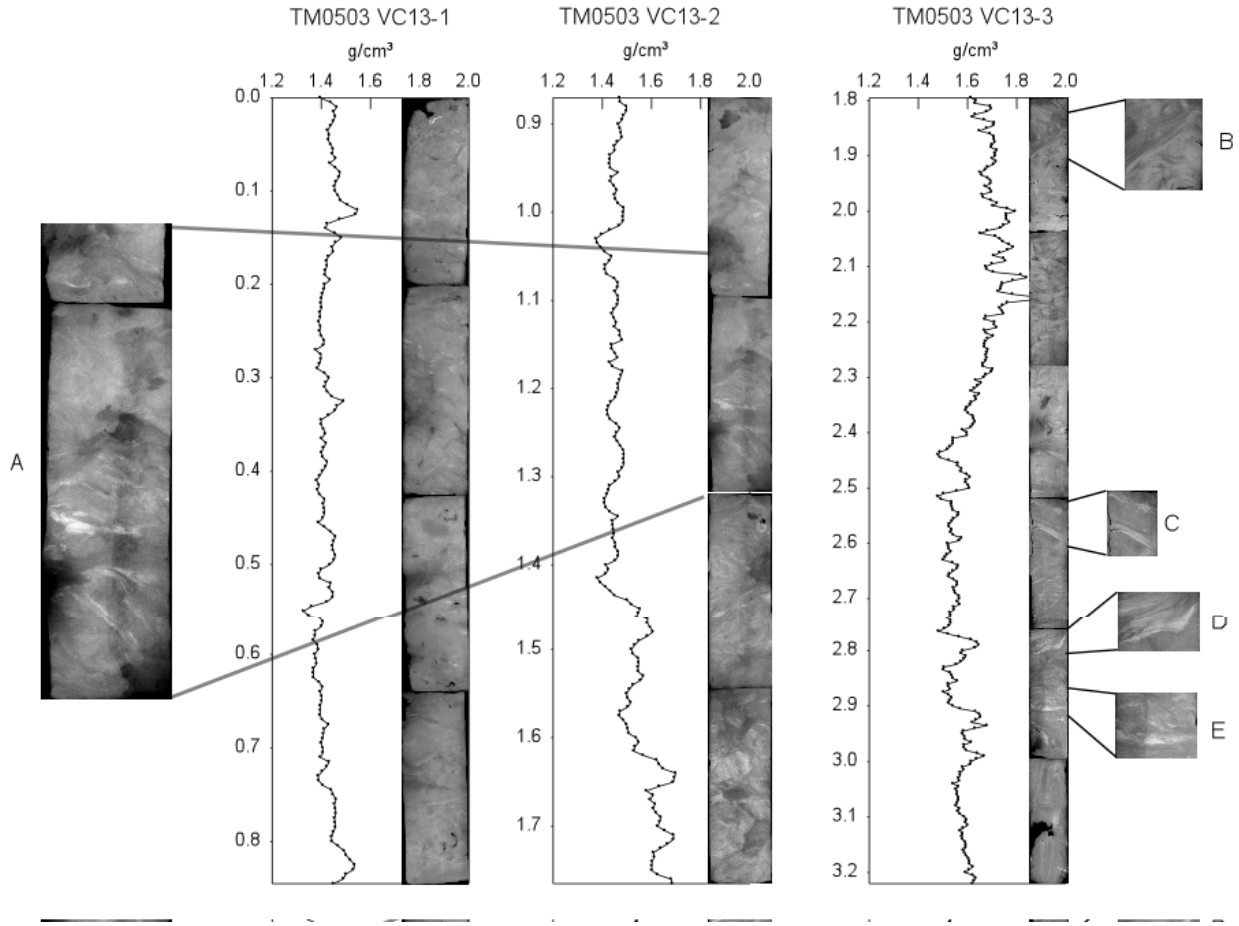

Figure 25. Gamma bulk density and x-radiographs for TM0503 VC13. Section 3 is at a different scale than section 1 and 2.

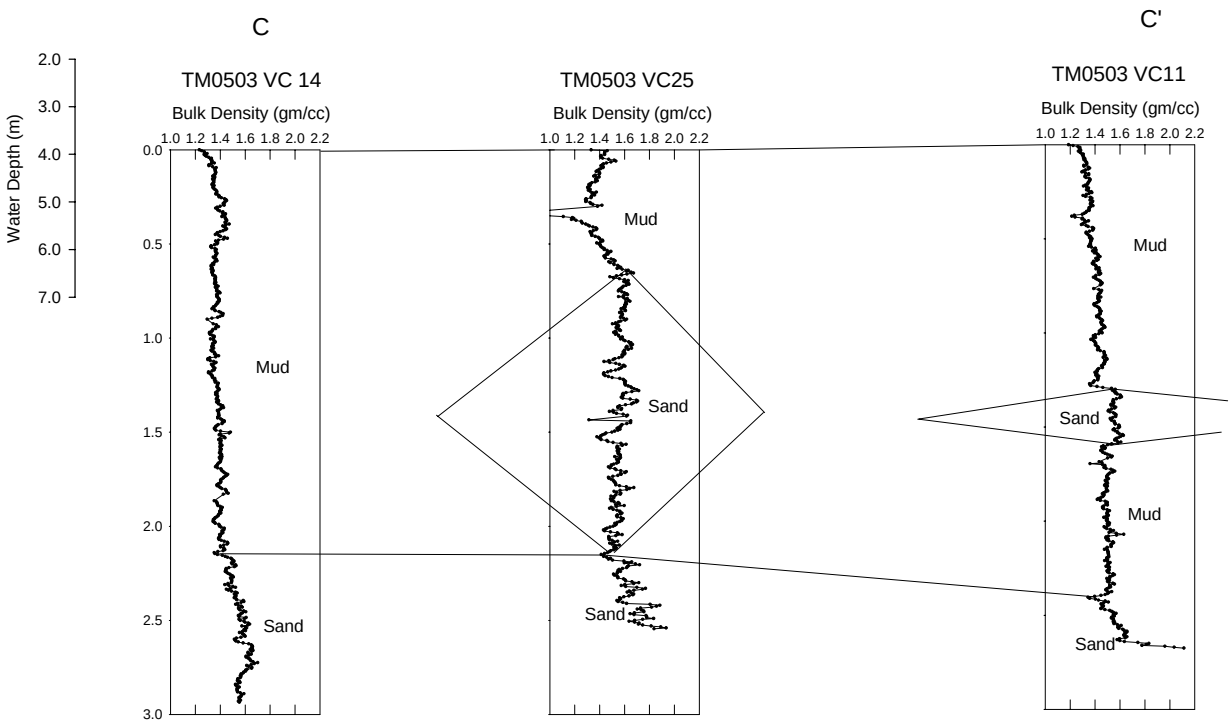

Figure 26. Cross section C to C’ is an East to West cross section from vibracores VC14 – VC25-VC11.

of the core displays relatively low density (~1.4 g cm^{-3}); however, the density increases to ~1.6 g cm^{-3} between 0.5m and 0.7m. Between 0.7 m and 2.15 m bsf the bulk density decreases from 1.6 g cm^{-3} to 1.4 g cm^{-3}. Density maxima and minima occur as spikes in the profiles within this depth interval. The base of the core displays an increase in density to ~1.8 g cm^{-3}. Vibracore VC11, located 15 km to the east of VC25, displays a gradual increase in the gamma bulk density from ~1.25 g cm^{-3} to ~1.45 g cm^{-3} with depth. A 0.3 m interval between the depths 1.3 m and 1.6 m, displays an increased bulk density of ~1.6 g cm^{-3}. The base of the core displays an increase in bulk density with depth from ~1.4 g cm^{-3} to >1.8 g cm^{-3}.

Cross section D to D' (Fig. 2) is an east-west transect that encompasses vibracores VC24, VC2, VC10, and VC9 (Fig. 27). The average bulk density of these vibracores is above 1.6 g cm^{-3} , suggestive of sandy sediment. Vibracores VC2, VC10, and VC9 are all located north of Horn Island and display a region of elevated bulk density (~2.1 g cm^{-3} in VC2, ~1.9 g cm^{-3} in VC10, and ~2.1 g cm^{-3} in VC9) in the top ~1.0 m of the cores. Vibracore VC14 has a near constant bulk density of ~1.8 g cm^{-3} throughout the core.

Tropical Storm Isidore and Hurricane Lili

Three box cores (Fig. 2, Table 1) were collected after the passage of Tropical Storm Isidore and Hurricane Lili to determine the effects of these two storms on the sedimentary fabric of Mississippi Sound. The cores were subsampled for X-radiography, radiochemistry, and granulometry. The X-radiographs from box cores Est-1, Shelf-2, and Shelf-3 (Figs. 28, 29, 30) display variable sedimentary features. Box core Est-1 reveals two distinct zones separated by an undulating contact at ~5 cm. Above this contact, a mud drape overlain by coarse grained sediment is evident in the x-radiograph. Below the contact is bioturbated muddy sand. Box core Shelf-2 sedimentary fabric is bioturbated mud with shell fragments. Box core Shelf-3 is

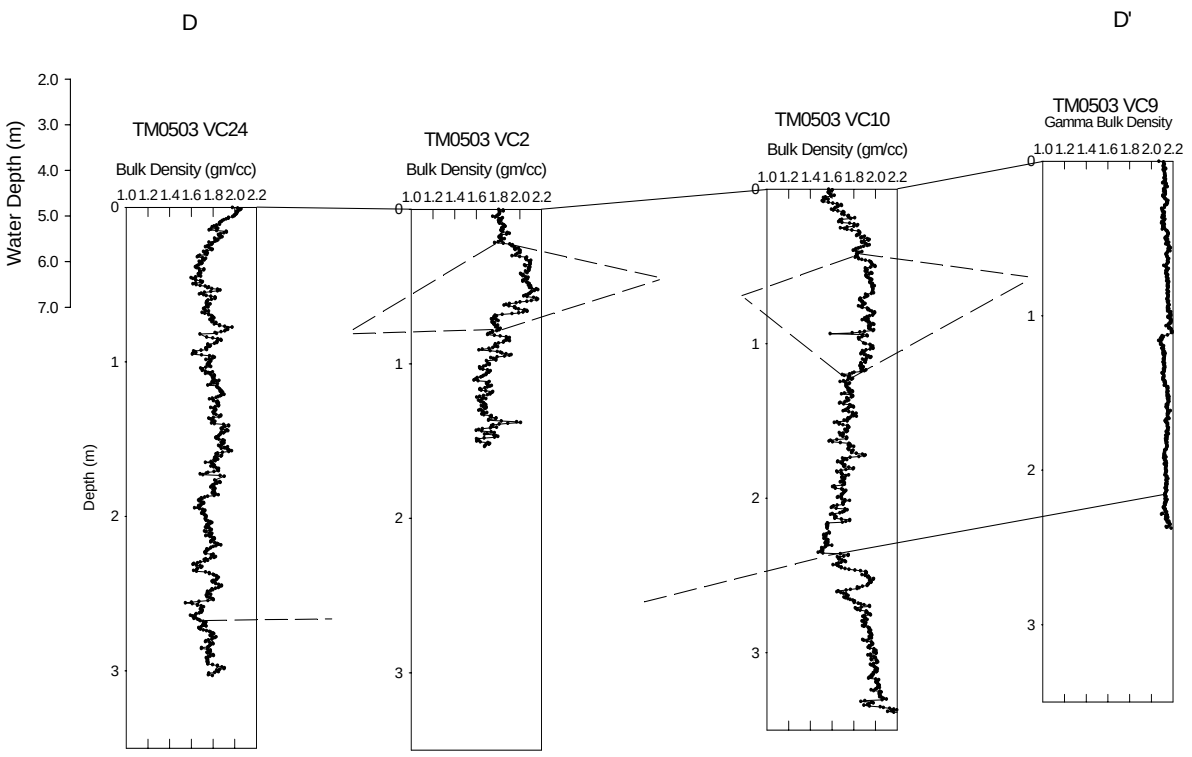

Figure 27. Cross section D to D'. Gamma bulk density profiles of VC24, VC2, VC10, and VC9.

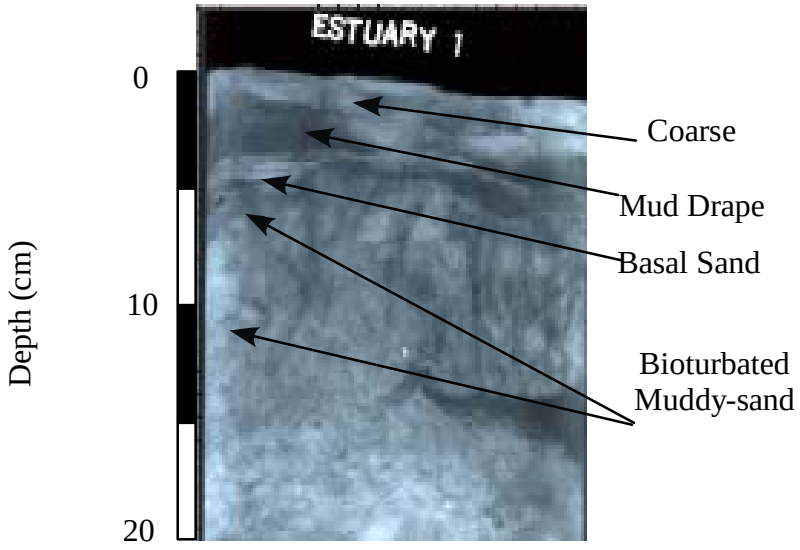

Figure 28. X-radiograph of Est-1 displays a basal sand layer overlain by a mud drape. The top of the x-radiograph displays coarse sediment and the base of the x-radiograph displays bioturbated muddy-sand.

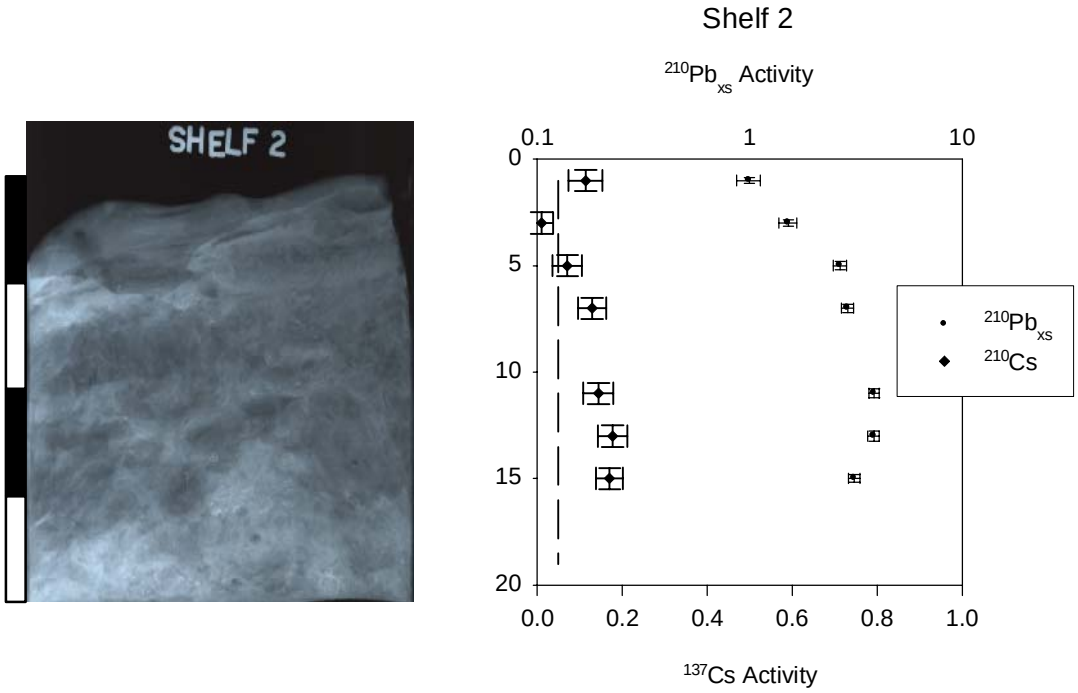

Figure 29. X-radiograph and radiochemistry for Shelf-2.

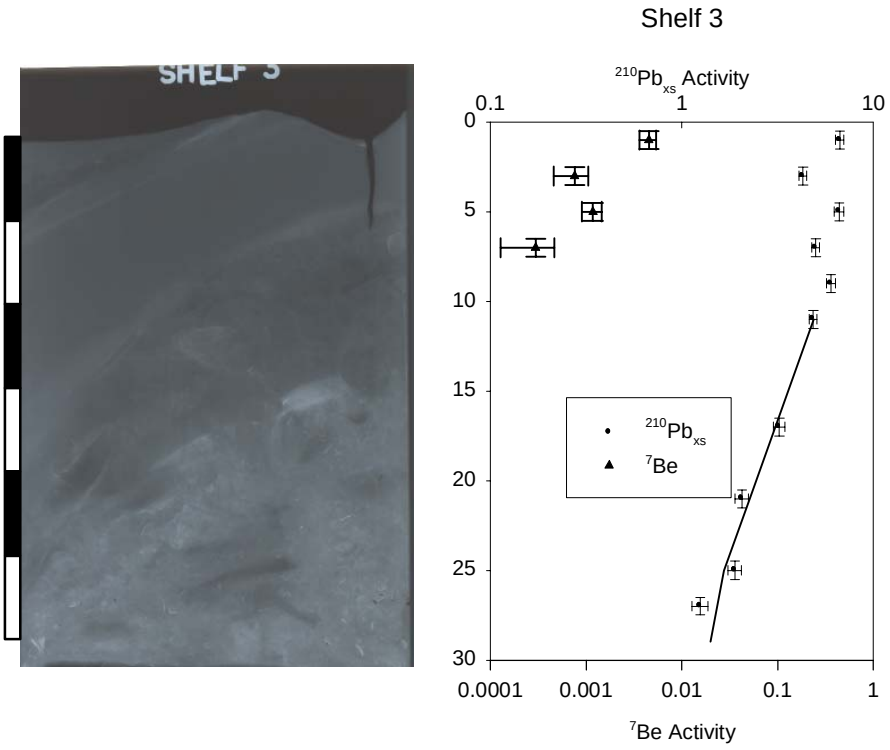

Figure 30. X-radiograph and radiochemistry for Shelf-3.

characterized by a mud layer ~10 cm thick, interbedded by two zones of coarse high-density material, overlying bioturbated muddy-sand.

Excess ^{210}Pb and ^{7}Be profiles were plotted for Shelf-1, Shelf-2, and Est-3 (Figs. 29, 30, 31). The upper ~5 cm of Est-3 displays a zone of constant $^{210}Pb_{xs}$ activity. Below this zone, the profile gradient can be attributed to sediment accumulation and radioactive decay. The ^{7}Be profile displays activity in the upper 6-8 cm, below which ^{7}Be is non-detectable. The $^{210}Pb_{xs}$ profile for Shelf-2 displays an unusual increase in activity with depth. There was also no ^{7}Be detected at this site. Box core Shelf-3 displays two different trends in the profile. The top 8-10 cm displays constant $^{210}Pb_{xs}$ activity. Below this zone the profile displays exponential decay associated with sediment accumulation and radioactive decay. The profile of ^{7}Be displays a penetration depth of ~7-10 cm below the surface (bsf) in Shelf-3.

Hydrodynamic data collected from CSI-13 and NDBC42007 were used to determine the wave conditions during these two storms and calculate the near bottom orbital velocities. Within Mississippi Sound, CSI-13 recorded a maximum significant wave height (H_s) (Fig. 32) detected for Tropical Storm Isidore of ~1.7 m, the mean wave period (T_{av}) (Fig. 33) of ~3.5 s, and the maximum water level (Fig. 34) recorded of ~8 m. During Hurricane Lili, H_s was ~1.2 m, T_{av} was ~ 3.5 s, and the maximum water level recorded was ~7.7 m. Storm surge was ~1.6 m during Tropical Storm Lili and ~0.6 m, during Hurricane Lili within Mississippi Sound. South of the barrier islands, NDBC 42007 recorded H_s for Tropical Storm Isidore and Hurricane Lili to be 4.9 m and 3.8 m respectively. Mean Peak wave period for the two storms was 13 s for both storms. Water level was not recorded by NDBC 42007. Wave fiction velocities within Mississippi Sound, calculated through Eq. 3 CSI-13 data, reached a maximum of ~0.05 m/s during Tropical Storm Isidore and ~0.05 m/s during Hurricane Lili. Wave friction velocities, calculated from EQ.

3 using NDBC-42007 data, on the shelf are >> 1 m/s for both Tropical Storm Isidore and Hurricane Lili.

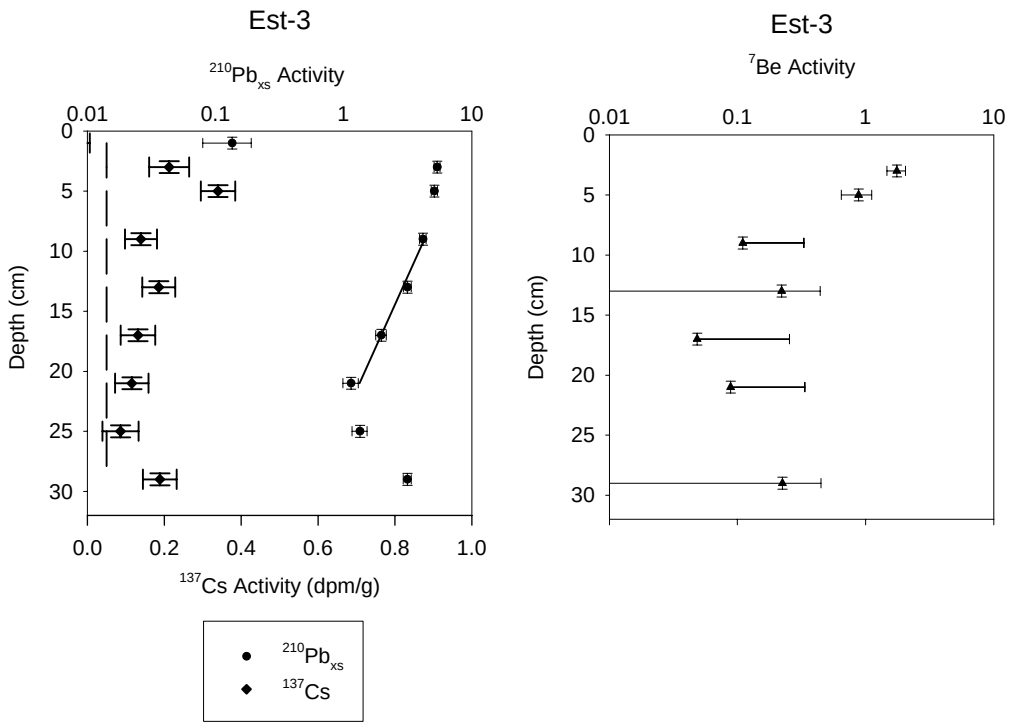

Figure 31. $^{210}Pb_{xs}$ activity, ^{137}Cs activity, and ^{7}Be activity for Est-3.

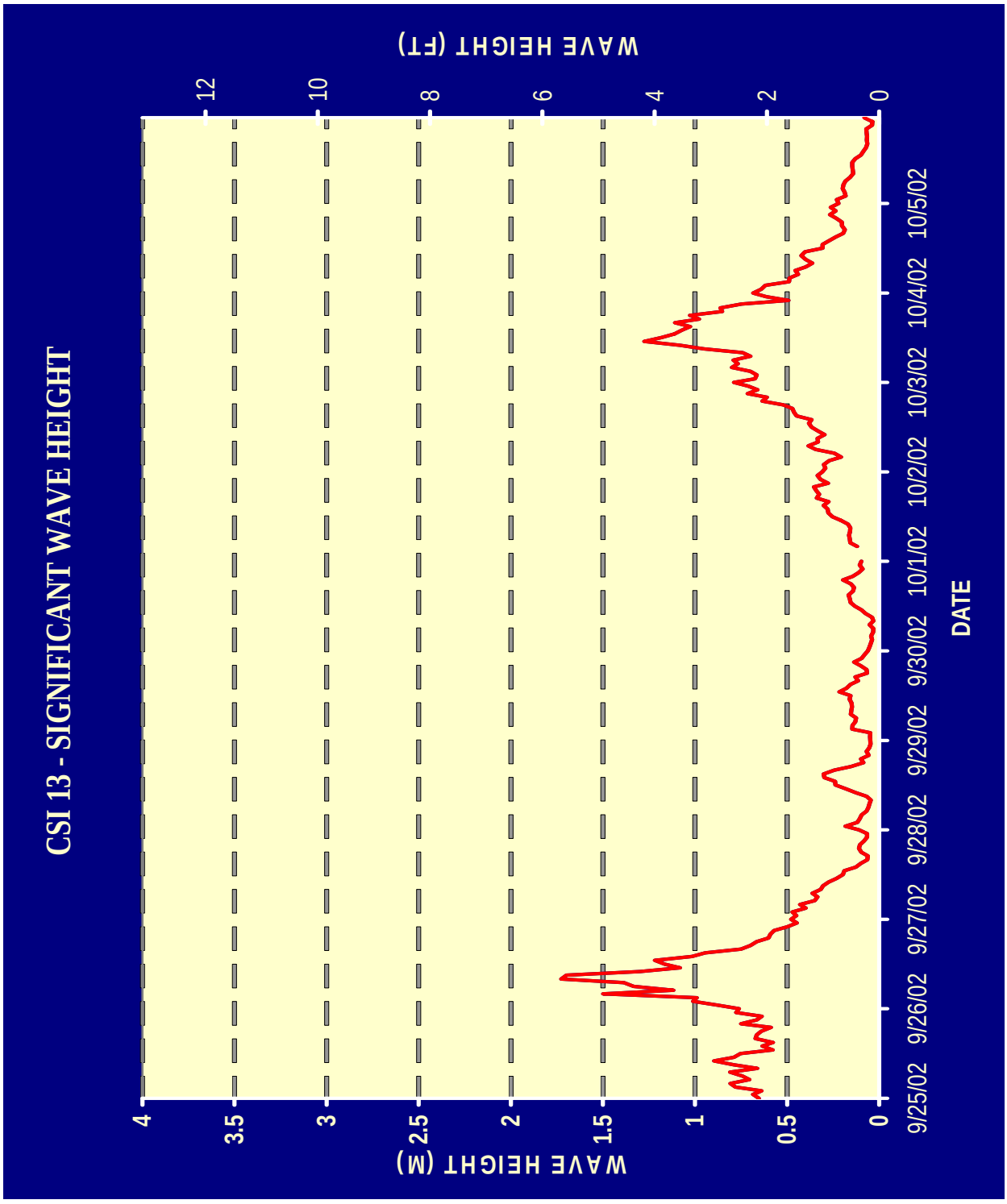

Figure 32. Significant wave height during Tropical Storm Isidore and Hurricane Lili at WAVCIS CSI-13 (LSU WAVCIS lab).

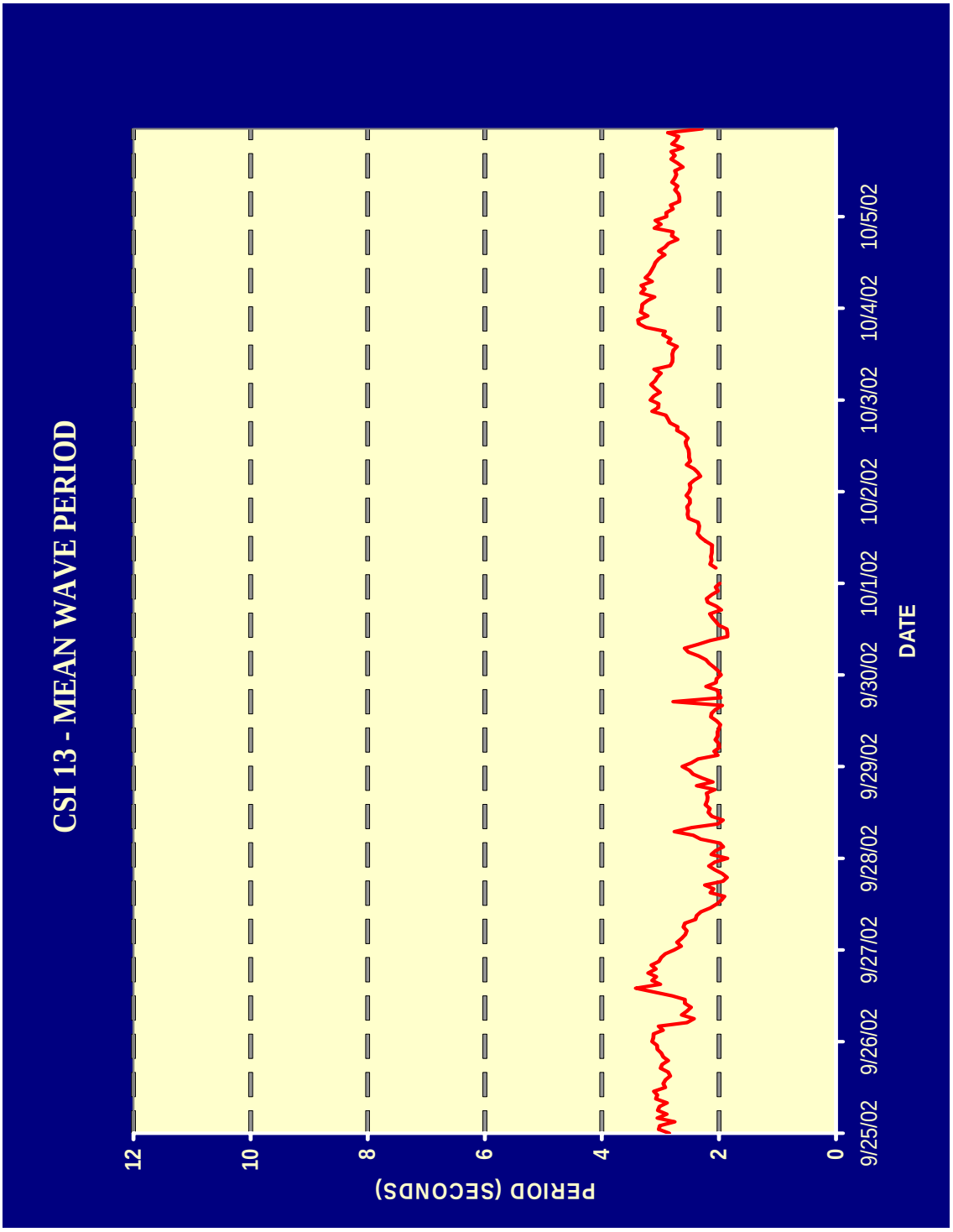

Figure 33. Mean wave period recorded at WAVCIS CSI-13 during Tropical Storm Isidore and Hurricane Lili (LSU WAVCIS Lab).

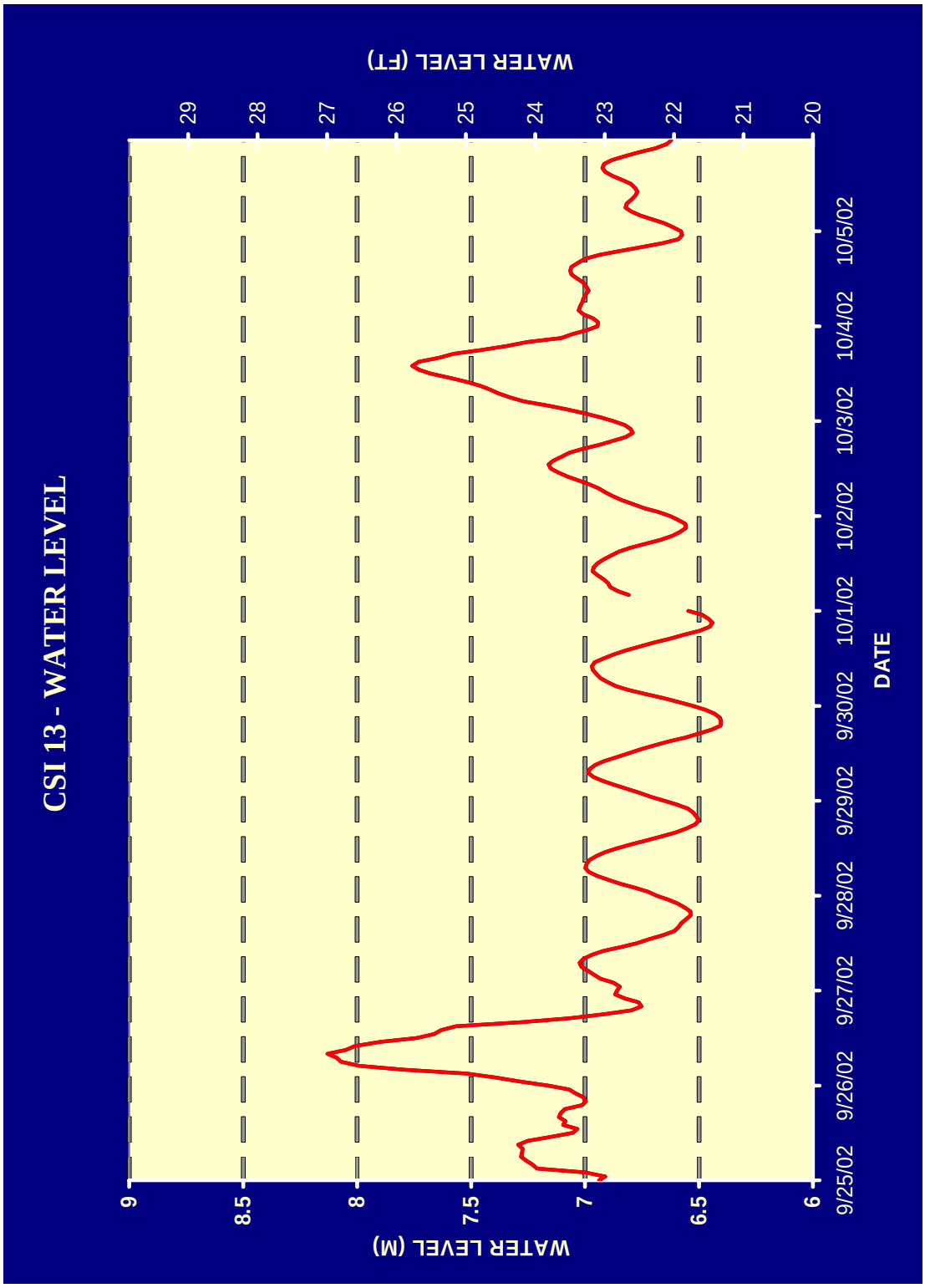

Figure 34. Water level recorded at CSI-13 during Tropical Storm Isidore and Hurricane Lili (LSU WAVCIS Lab).

Discussion

Sediment Facies and Hydrodynamics

Patterns of sediment deposition within Mississippi Sound are influenced by mean frequency, intensity, and duration of sediment resuspension and transport, and the proximity to sediment sources. Wright (1995) states that, over time, hydrodynamic regimes and morphologic patterns co-evolve. Therefore, the stratigraphic record preserves changes in the morphodynamic conditions (morphology + associated hydrodynamic behavior). Within inner-shelf environments, the near bed region is dominated by wave-boundary layers, which are strongly influenced by the amount of wave energy reaching the bed. Wave energy is a function of wave properties (period, wave height, and wave length) and water depth (Wright, 1995). Thus, changes in water depth (through either a rise or fall of sea level or infilling of the basin with sediment), or changes in the exposure to open ocean waves (through shoaling or barrier island migration) may change the hydrodynamic conditions within the Sound, and these changes may be recorded in the sedimentary record as changes in the sediment facies (Wright, 1995).

Water depth can be influenced by either changes in mean sea level, through the infilling of a basin with sediment, or both. Figure 35 displays the wave friction velocity (U_*) with respect to water depths, wave height, and wave period (calculated from EQ.3; Wright, 1995). With increasing depth, the wave friction velocity decreases for particular wave conditions. However, for a particular depth, the wave friction velocity increases with increased wave height and period. According to van Rijn (1984) initiation of motion for non-cohesive particles occurs when the shear velocity U_* equals the particle settling velocity. For example, the Stokes settling velocity for fine sand (100 μm) is 0.008 m s^{-1}; therefore, waves with heights greater than 1.2 m would have to exist for fine sand (100 μm) to be resuspended in water with a depth of ~4 m; however,

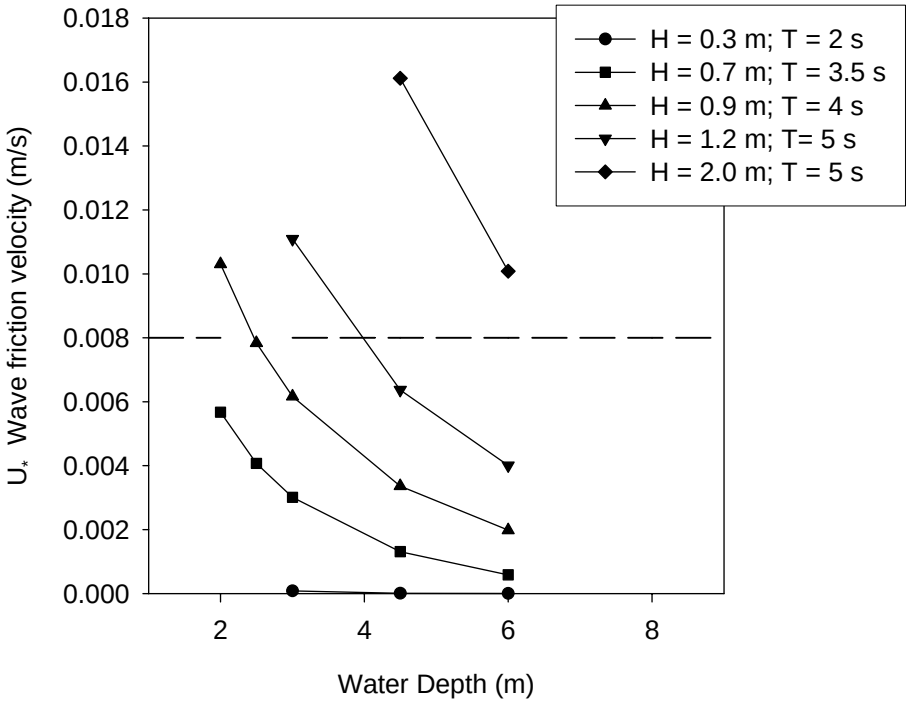

Figure 35. Plot of U_* for different water depths and wave parameters (wave height = H; wave period = T).

100 µm sand would not be resuspended in water depths > ~4 m with the same wave conditions. Thus, sediment deposited in deeper water (> 4 m) will not be as strongly influenced by wave action as sediments deposited in shallower water (< 4 m). Therefore, the deeper water depositional environment is more suited to the deposition of fine sediments (silt and clay) than the shallow water environment. This energy gradient influences grain size variations on the sea floor; resulting in the formation of multiple depth-related sedimentary facies.

Patterns of Recent Deposition

The St. Bernard Lobe of the Mississippi Delta (Fig. 36) was active between 4000 and 2000 years before present (Roberts, 1997). The construction of the St. Bernard subdelta cut off Mississippi Sound from the open Gulf of Mexico, resulting in reduced wave energies east of Cat Island, and allowed for the formation of the characteristic north-south spit (Otvos, 1976 and 2004). Discharge from the St. Bernard lobe combined with runoff from the Pearl River, diluting nearshore Gulf of Mexico water, and reducing salinities (Otvos and Giardino, 2004). With the abandonment of the St. Bernard lobe and the subsequent destruction of the delta beginning ~2000 yr bp, the Western Sound was exposed to the open Gulf of Mexico and to increased wave energy (Otvos, 1976; Otvos and Giardino, 2004). Therefore, patterns of recent estuarine sedimentation in the western Sound have only been active in the last 1500 – 2000 years, since the abandonment of the St. Bernard lobe of the Mississippi delta. Based on ^{14}C geochronology, ~2000 ybp is comparable to the age of the oldest Holocene sediments collected for this study.

The X-radiographs of box cores display laminations of mud and sand in the top 5 cm (Figs. 3, 4, 5, and 6), which are representative of physical reworking due to wave action. Below this depth, the sedimentary fabric is generally more intensely bioturbated. Excess ^{210}Pb profiles of BC3 and BC12 display near constant activity in the upper 10-12 cm. Homogenization of

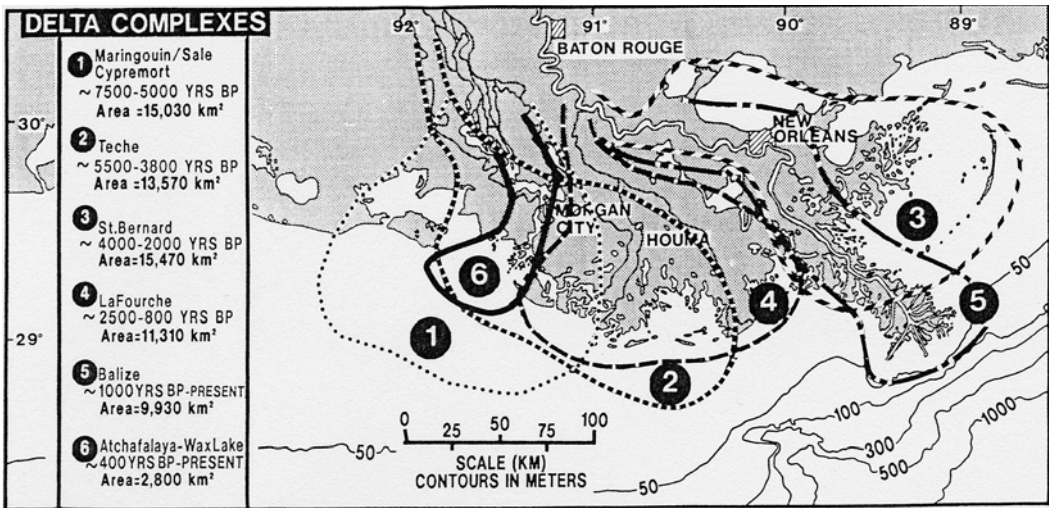

Figure 36. Location map of Mississippi River delta complexes (Adapted from Roberts, 1997).

particle-bound radioisotopes, through mixing by physical and biological processes, can result in a reduced gradient in radioisotope activity with depth (Bentley et al., 2002). Below this depth, both cores display depth-dependent gradients that are associated with radioactive decay and sediment burial. In a study conducted by Bentley et al. (2002), the authors concluded that physical and biological mixing are important processes that occur in the top of the seabed. These conclusions are supported by the presence of physically stratified sediments top 4-5 cm bsf of cores collected during this study and through ^{7}Be measurements made after the tropical storms. Thus, when sediment is first deposited on to the seafloor, it undergoes both physical and biological reworking in the top 4-5 cm of sediment layer. Below this depth, biological activity dominates, resulting in the destruction of sediment stratification through bioturbation. Excess ^{210}Pb profiles of box cores display zones of near constant activity at the top of the cores. This zone of near constant activity extends to depths of 10-12 cm bsf, suggesting that the depth of active bioturbation is 10-12 cm. Bentley et al. (2000) calculated a depth of rapid bioturbation in the study area to be <5-7 cm below the sea surface and a depth of biogenic mixing of ~10 cm below the sea surface.

Between 18-24 cm, BC 12 displays a zone of near constant activity in the ^{210}Pb profile. This depth corresponds to the sandy layer displayed in the X-radiograph and reflected in the grain size data (Fig. 6). Studies into the preservation potential of major hurricanes within Mississippi Sound, Bentley et al. (2000, 2002), concluded that Hurricane Camille did produce a recordable event layer in the sedimentary record. The depth of the layer present in BC12 is deeper (22-26 cm below the seafloor) than those reported by Bentley et al. (2002) (10-15 cm below the seafloor); however, sediment accumulation rates are variable throughout Mississippi Sound and BC12 is located ~25 km to the west of Bentley's 2002 study area. The accumulation

rates calculated for BC12 (0.41 cm yr^{-1}) are higher than the 0.31 cm yr^{-1} rate published by Bentley et al. (2002). Therefore, it is possible that the site where BC12 was collected experienced more rapid accumulation, burying the event layer more deeply than at the locations studied by Bentley et al. (2002).

Impacts of Tropical Systems

Bulk density data collected for KJ0601 GC 10 reveals eight peaks in the bulk density that exceeded ~1.6 g cm^{-3} (Fig. 8), increases in bulk density have been shown to correspond to increases in sand content in VC26 and VC28 (Figs. 21 and 19). The peaks in bulk density also correspond to sandy layers displayed in the X-radiographs (Fig. 8). Similar sandy features observed in gravity and box cores collected in Mississippi Sound have been interpreted to be event layers deposited by major hurricanes (i.e. Hurricane Camille, 1969; Bentley et al., 2000; 2002). Therefore, peaks in the gamma bulk density of GC10 are possible sandy basal portions of event layers recorded in the sedimentary fabric. Corrected and calibrated ^{14}C dates from shells collected from GC10 reveal a maximum age of 758 years BP at a depth of 2.61 m. Assuming that at least 6 of the peaks observed in the MSCL data are in fact event layers, this yields a return frequency of one recordable storm event every ~125 years. Thus, using the bulk density profile, we estimate that at least 8-26% of the sediment column was deposited by recordable storm events in the Western Mississippi Sound. Smaller storm events and typical estuarine processes deposited the other 74 – 92% of the sediment column.

Wave data indicate that Tropical Storm Isidore created a more intense environment for sediment resuspension than Hurricane Lili. Orbital velocities were also much higher south of the barrier islands on the inner shelf than within Mississippi Sound. Radioisotope and X-radiography data indicate the formation of a variable event layer ~ 1-4 cm thick within Mississippi Sound.

South of the barrier islands there is very little deposition on the inner shelf; however, further offshore the data indicate the deposition of a 10 cm thick event layer, which indicates that the shelf experienced intense erosion nearshore and rapid deposition further offshore. Thus, Tropical Storm Isidore had a greater impact on the region than Hurricane Lili. This impact was greater south of the barrier islands on the inner shelf. However, the event layers left behind are not sufficient to survive the typical estuarine and biological conditions that are active today.

Subsurface Facies

A series of lithofacies groups are identified within the vibracores and gravity cores based on grain size, composition, sedimentary texture, and sedimentary structures. Three lithofacies were identified from the vibracores: low-energy muddy facies, high-energy sandy facies, and pre-Holocene. The muddy facies is composed of greater than 50 percent mud. The sedimentary fabric is intensely bioturbated; however, lenses of sand and silt are present. Some shell fragments and whole shells are present. The sandy facies is composed of greater than 50 percent sand and silt, with an abundance of shells and shell fragments. This facies is interpreted as a transition from beach facies to open bay muddy facies. Sediments that are stiff, hard, and more compacted than the overlying Holocene sediments characterize the pre-Holocene/Pleistocene facies. The composition of these sediments ranges from clay, silty-clay, sandy-clay, and in some cases sand (Fisk and McClelland, 1959; Katuna et al., 1964; Ludwick, 1964; Bernard et al., 1970; Coleman and Prior, 1980).

Deposition Around the Barrier Islands

Otvos and Giardino (2004) created a conceptual model of barrier island evolution in association with delta development. This model was based upon the evolution of the St. Bernard lobe of the Mississippi Delta and its effects on the barrier islands of the western Mississippi

Sound (Fig. 37). Progradation of the St. Bernard delta gradually buried proximal members of the barrier island chain, and interrupted the sand supply from littoral drift and onshore transport from the inner shelf. This resulted in the erosion and eventual elimination of some islands, such as the Square Handkerchief Shoal (which is probably a degraded barrier island), and the partial erosion of Cat Island (Otvos and Giardino, 2004).

A north – south cross section north of Cat Island records the progradation of the northern spit of Cat Island as well as the evolution of the depositional environment north of Cat Island (Fig. 18). The cross section displays the sandy sedimentary facies of VC26 prograding onto the muddy facies of vibracores VC27 and VC28. The bases of VC27 and VC28 record a sandy sedimentary facies at depth of ~1.8 m bsf and ~1.3 m bsf respectively. From the assumption that the sandy sediment facies was deposited in more open waters with increased wave energy, deposition of this sandy facies occurred before the northern spit of Cat Island began to influence the depositional environment of the region, when the region was open to the Gulf of Mexico and increased wave energy. Utilizing the apparent sediment accumulation rate for VC28, 0.2 cm yr^{-1}, it is estimated that this region began to become shielded by the formation of the Cat Island spit between ~750 yrs BP and ~1000 yrs BP, approximately 500 to 700 years after the abandonment of the St. Bernard delta. Prior to this time, wave energy was higher due to open water and the environment was not conducive to the deposition of fine-grained silts and clays. With the formation of the northern spit of Cat Island the depositional environment evolved from an open water environment to closed water environment that is present today at core locations VC27 and VC28.

Cross section B-B’ stretches the north to south just north of West Ship Island. Core VC12 consists entirely of the nearshore facies sediments whereas, the nearshore facies in only present

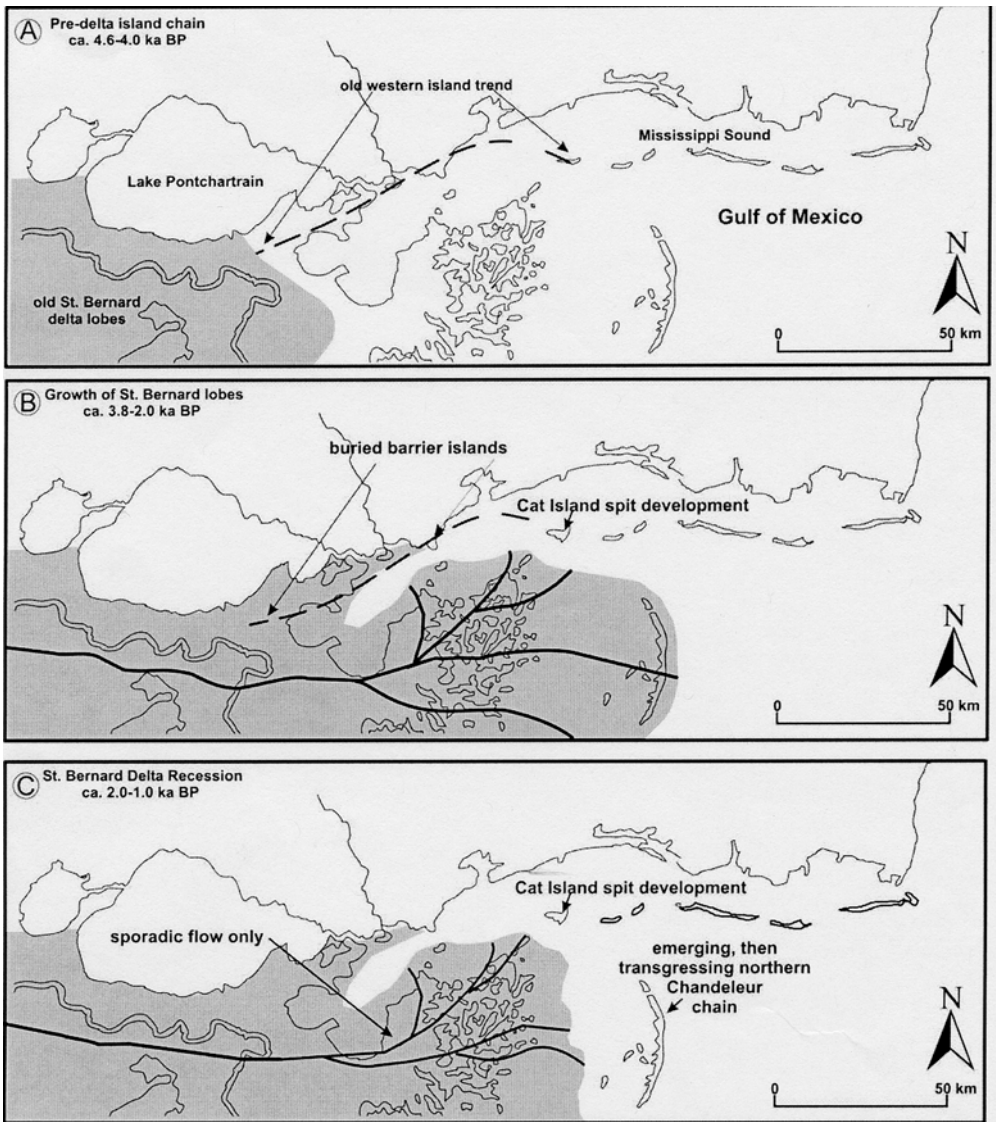

Figure 37. Model of a barrier island chain and associated delta plain development (adapted from Otvos, 2004).

at the base of vibracores VC14 and VC13. The open bay facies characterizes the tops of VC14 and VC13. The cross section in Figure 23 thus records the evolution of the depositional environment from the shallow water, near shore environment to the deeper water, open-bay environment in core VC13 and VC14. However, due to the close proximity of VC12 to Ship Island, sediment deposition at VC12 is controlled by sand transport from Ship Island into the Sound.

Located just north of the western tip of Horn Island, TM0503 VC2 documents the migration of Horn Island, as well as changes in the local hydrodynamics with the westward migration of the island (Fig. 10). The base of the core (0.9 m to 1.5 m) is composed of greater than 50% sand, whereas the top 0.96 m of the core is greater than 50% mud; there is also an increased percentage of shell hash in the top 0.96 m, which is visible in the x-radiographs. The Mississippi barrier islands are migrating through westward littoral drift of barrier island sand. Cipriani and Stone (2001) calculated that sand is transported along the western tip of Horn Island at a rate of ~24,000 $m^3 yr^{-1}$. Analysis of the coarse grained fraction of VC2 reveals that the mean grain size of the sediment is ~250 μm, which is characteristic of the Mississippi barrier islands (Cipriani and Stone, 2001). However, there is a coarsening upward trend in the coarse sand fraction from ~1.4 m bsf to ~0.5 m bsf. This trend may be recording the migration of the barrier island, and an increase in deposition of foredune sand from the barrier island. Bentley et al. (2002) modeled the bottom currents between Horn Island and East Ship Island generated by Hurricane Camille in 1969. The model suggested a northward flow as storm surge increased. This flow pattern produced currents up to 2 m s^{-1} and persisted for less than 6 hours. The model also predicted topographic steering around the islands. After the storm surge peak, bottom currents reversed direction and flowed south into the open Gulf of Mexico with similar velocities

as the northward flow. Rucker and Snowden (1988) state that, " Incursions of cold fronts play an important role in the sedimentary processes of the barrier island system." The conditions present during the passage of tropical cyclones and the more frequent cold fronts allow for the erosion of shell material from the islands to be deposited along the tips of the islands, which allows for the more frequent deposition of shell and sand along the tip of Horn Island. Therefore, as Horn Island migrated westward, the availability of barrier island sand for deposition increased with time until the barrier migrated past the core location, at which time, the deposition of sand decreased and the deposition of shell and shell hash from the barrier island increased.

Facies Trends in the Central Mississippi Sound

Facies trends within the central Mississippi Sound are portrayed in two parallel cross sections, C-C' and D-D', Figure 2. The vibracores in cross section C-C' display near constant gamma bulk density values throughout most of the cores; however, at the base of the cores (2.15 m for VC14 and VC25, and 2.4 m for VC11) the cores display increasing bulk-density values with depth (Fig. 26). Bulk density values greater than 1.6 g cm^{-3} have been shown to correspond generally to sand content equal or greater than 50% in cores VC26, VC13, and VC2; therefore, it is likely that the high bulk density values in VC14, VC25, and VC11 are attributable to an increase in sand content. The higher energy sandy facies is defined by sediment with greater than 50% sand content; therefore, the bulk density of vibracores VC14, VC25, and VC11 may suggest the evolution from deposition of the sandy facies within a higher energy environment to the deposition of muddy sediment within a lower energy environment. Two factors that influence the wave dynamics within Mississippi Sound are changes in water depth and exposure to the open Gulf of Mexico. Wind speed, direction, and intensity influence wave formation, but peak storm-generated wind fields are likely to have remained similar over the past few centuries. Current

water depths along this transect range from ~3.2 m to ~5.7 m. From the plot of U_* and water depth (Fig. 35), a 0.9 m wave with a period of 4 s would be create a U_* of ~0.006 m/s, which would not resuspend 100 µm sand. Decreasing water depth from 3 m to 2.5 m would increase the shear velocity from, ~0.006 m/s to 0.008 m/s, which is necessary to resuspend the sand. Therefore, by lowering water depth by ~0.5 m, the hydrodynamics would allow for the resuspension of 100 µm sand. However, variations in water depth are controlled by both sediment accumulation and changing sea level. Assuming an average accumulation within Mississippi Sound during that past ~1000 years of ~0.3 cm yr^{-1}. For constant sea level water, depth would have been up to ~ 3 m deeper than present approximately 1000 yr bp. Present rate of sea level rise is ~0.1 cm yr^{-1}(Penland and Ramsey, 1990). Thus, by combining the estimated sediment accumulation and the estimated rise in sea level, water depth would have been ~ 2 m deeper than present day conditions. Thereby, creating conditions that may be favorable for a lower energy environment and the deposition of a muddy sedimentary facies. However, because variations in rates of sea level change and accumulation are not well known, this represents only one possible scenario. Hydrodynamic conditions are also influenced by exposure to the open Gulf of Mexico. Along the Mississippi – Alabama shelf, the transition from mud to sand occurs at ~ 12 m water depth (Sawyer, 2001), which suggests greater wave energy in the open Gulf of Mexico can affect the deposition of sedimentary facies in deeper waters. Figure 35 displays that in water depth of greater than 6 m; waves with heights of 2 m and periods of 5 s will create boundary layer conditions that are suitable for the resuspension of fine sand. Therefore, by exposing Mississippi Sound to increased wave energy from the Gulf of Mexico, conditions may become favorable for the deposition of the higher-energy sandy facies in the relatively deeper waters of Mississippi Sound. Exposure to the open waters of the Gulf of Mexico may be the

result of barrier island migration and the passes between the barrier islands. Thus, the bases of these cores may be recording the final stages of the barrier island migration and the reduction of wave energy from the open Gulf of Mexico.

Cross section D-D' is located south of cross section C-C' and is located just north of Horn Island. The vibracores have higher bulk density values (~1.75 g cm^{-3} to 2.2 g cm^{-3}) than those displayed in C-C' (VC14, VC25, and VC11 which have bulk density values that range from ~1.2 g cm^{-3} to 1.65 g cm^{-3}), and increases in bulk density have been shown to correspond to increases in sand content in VC26 and VC28 (Figs. 21 and 19). Therefore, it is assumed that the cores in D-D' have higher sand content within their sediments than C-C'. Analysis of the coarse grain size fraction in cores with higher bulk densities (VC2, and VC15 and VC16 in the eastern Mississippi Sound) reveals that the average mean grains size is ~250 μm, which is characteristic of Mississippi barrier island mid-tide level sands (Cipriani and Stone, 2001). The average water depth within cross section D-D' (~4.5 m) is greater than the average water depth of cross section C-C' (~4 m); however, the distance from the islands to the cores is much less for D-D' (< 1m) than for cross section C-C' (> 3.5 m). Therefore, cores located in closer proximity to the barrier islands probably received a greater percentage of their sediments from the barrier islands, than cores located in the more central regions of the Sound.

Holocene / Pleistocene Contact

The bases of vibracores VC15, VC17, and VC18 are characterized by a sharp contact with a compacted greenish gray silty-clay. Previous studies in Mississippi Sound have determined that the late Pleistocene sediments underlying the recent Holocene sediments is stiff, hard, and more compacted. The composition of these sediments ranges from clay, silty-clay, sandy-clay, and in some cases sand (Fisk and McClelland, 1959; Katuna et al., 1964; Ludwick,

1964; Bernard et al., 1970; Coleman and Prior, 1980). Therefore, cores VC15, VC17, and VC18 may be penetrating through the Pleistocene/Holocene boundary into the compacted Pleistocene clay.

Studies have suggested that the Pleistocene surface in Mississippi Sound dips to the southwest (Curry and Moore, 1963; Ludwick, 1964; Rainwater, 1964; Carroll, 1982). Ludwick's 1964 study of Mississippi Sound produced a contour map of the Pleistocene surface and calculated the slope of this surface to be 0.6 to 0.9 m km^{-1} (Fig. 38) to the south, with the depth as shallow as 3.5 m just south of Grande Batture and as deep as 18 m south of Horn Island. Rainwater's (1964) north south cross-section between Beauvoir and Ship Island maps the Pleistocene surface to be an irregular surface that dips to the south (6 m at Beauvoir to 15 m below Ship Island). Carroll (1982) conducted a study of in Mississippi Sound, and encountered the Pleistocene at shallower depths (6 to 7.5 m below the sea surface) in cores collected closer to Horn Island than cores collected closer to mainland Mississippi. The only cores collected for this study to penetrate through the Holocene/Pleistocene contact were VC15, VC17, and VC18, which were all collected in the eastern Mississippi Sound, which suggest that the Pleistocene contact is shallower in the eastern Sound and dips to the west. The depth at which TM0503 VC15 and VC17 penetrated the Pleistocene is 2.4 m and 2.0 m respectively. TM0503 VC18 had a shallow penetration depth of ~0.7 m before reaching a dense Pleistocene clay.

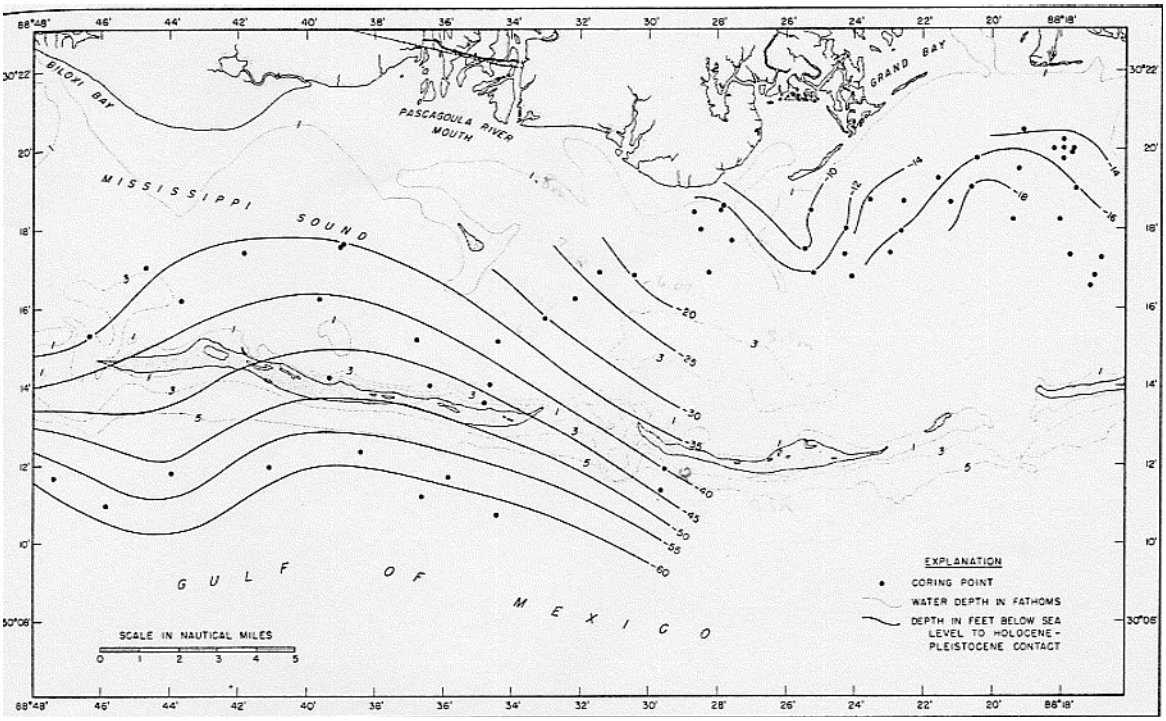

Figure 38. Contour map of the Holocene – Pleistocene contact in eastern Mississippi Sound and offshore (Ludwick, 1964).

Conclusion

Through a study of the physical and geochemical properties of sediments collected in cores throughout the western, central, and eastern Mississippi Sound, a general geochronology of the sedimentary deposition and facies evolution was constructed over the past 1000 years. The sediments within Mississippi Sound compose a complex depositional system that has responded to changes in sea level and hydrodynamics. This study has resulted in four main conclusions regarding the late Holocene deposition within Mississippi Sound:

1) Physical processes are active in reworking the sediment in the top 5 cm of the sea-bed; however, biological processes continuously rework the sediment to a depth of 10-12 cm resulting in the destruction of most stratification through bioturbation.
2) The migration of the barrier islands is being recorded in the sedimentary record as shallow water, sandy near shore facies overlying the deeper water, open bay muddy sedimentary facies.
3) Hydrodynamic and morphodynamic conditions within the Sound may be recorded in the sedimentary record as changes in the sediment facies. For example, the southern extent of the Sound behind Horn Island receives a greater percent of its sediment from the barrier island than do regions to the north.
4) Tropical systems regularly impact the region with varying intensity, size, and duration. These storms can impact the sedimentary fabric so that they are recorded and sandy event beds within a muddy matrix. Approximately 8-26% of the sediment column was deposited by recordable storm events in the Western Mississippi Sound, whereas smaller

storm events and typical estuarine processes deposited the other 74 – 92% of the sediment column.

References

Appleby, P.G., Oldfield, F., 1978. The calculation of ^{210}Pb dates assuming a constant rate of supply of unsupported ^{210}Pb to the sediment. Cantena 5, 1-8.

Bentley, S.J., Furukawa, Y., Vaughan, W.C., 2000. Record of event sedimentation in Mississippi Sound. Transactions – Gulf Coast Association of Geological Societies, 715-723.

Bentley, S.J., Keen, T.R., Blain, C.A., Vaughan, W.C., 2002. The origin and preservation of a major hurricane bed in the northern Gulf of Mexico: Hurricane Camille, 1969. Marine Geology 186, 423-446.

Bernard, H.A., Major, C.F., Parrott, B.S., Leblans, R.J., 1970. Recent sediments of southeastern Texas: a field guide to the Brazos alluvial and deltaic plains and the Galveston barrier island complex, Guidbook #11: University of Texas, Auston, 16pp.

Carroll, H.C., 1982. Lithologic and seismic determination and correlation of depositional environments in central Mississippi Sound [M.S. Thesis]: Oxford, Mississippi, University of Mississippi, 54pp.

Cipriani, L.E., Stone, G.W., 2001. Net longshore sediment transport and textural changes in beach sediments along the southwest Alabama and Mississippi barrier islands, U.S.A.. Journal of Coastal Research, 17, 443-458.

Coakley, J.P., Syvitski, J.P.M., 1991. Sedigraph technique: In: Syvitski, J.P.M (Ed.) Principles, Methods, and Application of Particle Size Analysis. Cambridge, Cambridge University Press, 368pp.

Coleman, J.M., Prior, D.B., 1980. Deltaic sand bodies- a 1980 short course education course note series #15: Tulsa. Oklahoma, American Association of Petroleum Geologists, 171pp.

Curray, J.R., 1965. Sediments and history of the Holocene transgression, continental shelf, northwest Gulf of Mexico,: In: Wright, H.E., Jr., and Frey, D.G., eds., The Quaternary of the Untied States: Princeton, New Jersey, Princeton University Press, pp.723-735.

Curray, J.R., Moore, D.G., 1963. Facies delineation by acoustic-reflection: northern Gulf of Mexico: Sedimentology, v.2, pp.130-148.

Eleuterius, C.K., 1977. Location of Mississippi Sound oyster reefs as related to salinity of bottom waters during 1973-1975. Gulf Research Reports, v.6., No.1, pp.17-23.

Eleuterius, C.K., 1978. Geographical definition of Mississippi Sound. Gulf Research Reports, v.2., No.2, pp.179-181.

Feng, H., Cochran, J.K., Hirschberg, D.J., 1999. ^{234}Th and ^{7}Be as tracers for the transport and dynamics of suspended particles in a partially mixed estuary. Geochimica et Cosmochimica Acta, 63, 17, pp 2487-2505.

Fisk, H.N., McClelland, B., 1959. Geology of continental shelf off Louisiana: its' influence onoffshore foundation design: Bulletin of Geological Society of America, v.70, pp.1369-1394.

Goldberg. E.D., 1963. Geochronology with ^{210}Pb. Radioactive Dating. Conference Proceedings, November 19-23, 1962. Athens, IAEA, pp.121-131.

Hoyt, J.H., 1967. Barrier island formation: Geological Societies of America Bulletin, v.78, pp.1125-1136.

Hummell, R.L., Parker, S.J., 1995. Holocene Gologic History of the Mississippi Sound, Alabama. Geologic Society of Alabama, 91pp,

Kahn, J.H., 1978. The role of hurricanes in the long-term degradation of a barrier island chain: Chandeleur Islands, Louisiana [M.S. Thesis]: Baton Rouge, Louisisana, Louisiana State University, 99pp.

Katuna, M.P., Ingram, R.L., 1974. Sedimentary structures of a modern lagoonal environment: Pamlico Sound, North Carolina: Raleigh, North Carolina, University of North Carolina, Sea Grant Program, Sea Grant Publication UNC-SG-74-14, 122pp.

Ludwick, J.C., 1964. Sediments of the northeastern Gulf of Mexico. In: Miller, R.L., (ed.), Papers in Marine Geology: Shepard Commemorative Volume: MacMillan: New York, p. 204-238.

McCave, I.N., Syvitski, J.P.M., 1991. Principles and methods of geological particle size analysis: In: Syvitski, J.P.M (Ed.) Principles, Methods, and Application of Particle Size Analysis. Cambridge, Cambridge University Press, 368pp.

Milne, I.H., Shott, W.L., 1958. Clay mineralogy of recent sediments from the Mississippi Sound area: Fifth National Conference on Clays and Clay Minerals, Publication 566, pp.253-265.

Muller, R.A., Stone, G.W., 2001. A climatology of tropical storms and hurricane strikes to enhance vulnerability prediction for southeast U.S. coast. Journal of Coastal Research, 17, 4, pp 949-956.

Neumann, C.J., Jaruinen, B.R., Pike, A.C., 1988. Tropical cyclones of the North Atlantic Ocean 1871-1986: Ashville, North Carolina, National Climatic Data Center, 186 pp.

Nittrouer, C.A., Sternberg, R.W., Carpenter, R., Bennett, J.T., 1979. The use of ^{210}Pb geochronology as a sedimentological tool: Application to the Washington continental shelf. Marine Geology 31, 297-316.

Nittrouer, C.A., Sternberg, R.W., 1981. The formation of sedimentary strata in an allochthonous shelf environment: the Washington continental shelf. Marine Geology 42, 201-232.

Noller, J.S., 2000. Lead-210 Geochronology, In: Noller, J.S., ed., Quaternary Geochronology: Methods and Applications, pp 115-120.

Otvos, E.G., 1970. Development and migration of barrier islands, northern Gulf of Mexico. Geological Society of America Bulletin 81, pp 241-246.

Otvos, E.G., 1973. Phase III: Sedimentology, cooperative Gulf of Mexico estuarine inventory and study, Mississippi : Gulf Coast Research Laboratory, pp 123-146.

Otvos, E.G., 1976. Post-Miocene geological development of the Mississippi-Alabama coastal zone: Journal of Mississippi Academy of Sciences, v. 21, pp 101-114.

Otvos, E.G., Giardino, M.J., 2004. Interlinked barrier chain and delta lobe development northern Gulf of Mexico. Sedimentary Geology 169, pp 47-73.

Penland, S., Ramsey, K.E., 1990. Relative sea-level rise in Louisiana and the Gulf of Mexico: 1908-1988. Journal of Coastal Research, 6, 2, pp 323-342.

Priddy, R.R., Crisler, R.M., Jr., Seliren, C.P., Powell, J.D., Burford, H., 1955. Sediments of Mississippi Sound and inshore waters: Mississippi Geological Survey Bulletin 82, 54 pp.

Rainwater, E.H., 1963. Late Pleistocene and recent history of Mississippi Sound between Beauvoir and Ship Island: Mississippi Geological Survey Bulletin. No. 103, pp 32-61.

Rucker, J.B., Snowden, J.O., 1988. Recent morphologic changes at Dog Keys Pass, Mississippi: The formation and disappearance of the Isle of Caprice: Transactions- Gulf Coast Association of Geological Societies, v. 38, pp 343-349.

Rucker, J.B., Snowden, J.O., Lambert, D.N., Kramer, K., 1990. Sub-bottom acoustic reconnaissance survey of sediments in eastern Mississippi Sound. In: Tanner, W.F. (ed.) Coastal Sediments and Processes. Proceedings, Ninth Symposium on Coastal Sedimentology. pp 101-111.

Sawyer, W., 2001. Mean Phi Map of Surficial Bottom Sediments for Mississippi Sound and the LA/MS Continental Shelf. http://www.navo.navy.mil/cgi-bin/graphic.pl/metoc/239/116/0-0-18/2, Draft 4/27/01.

Sommerfield, C.K., Nittrouer, C.A., 1999. Modern accumulation rates and a sediment budget for the Eel River Shelf: a flood-dominated depositional environment. Marine Geology 154, 227-242.

Sommerfield, C. K., Nittrouer, C. A., Alexander, C.R., 1999. ^{7}Be as a tracer of flood sedimentation on the Northern California margin. Continental Shelf Research 19, 335-361.

Trumbore, S.E., 2000. Radiocarbon Geochronology, In: Noller, J.S., ed., Quaternary Geochronology: Methods and Applications, pp 41-60.

Upshaw, C.F., Creath, W.B., Brooks, F.L., 1966. Sediments and microfaunca off the coast of Mississippi and adjacent states: Mississippi Geological Economic and Topographic Survey Bulletin No. 106, pp. 9-72.

Van Rijn, L.C.,1984. Sediment transport, Part I: Bed load transport. Journal of Hydraulic Engineering, v. 110, No. 10, pp 1431-1456.

Wright, L.D., 1995. Morphodynamics of Inner Continental Shelves. CRC Press, Inc., Boca Raton,FL, 241 pp.

Appendix A: Grain Size Analysis

TM0503 VC1			
Interval	Percent Sand	Percent Silt	Percent Clay
0-2	10.3	14.9	74.8
6-8	25.531	16.933	57.536
12-14	13.951	19.143	66.906
18-20	10.659	19.916	69.425
24-26	8.925	20.535	70.54
30-32	7.442	20.002	72.556
36-38	10.9	16.903	72.197
42-44	26.434	14.626	58.94
48-50	9.303	21.183	69.514
54-56	14.529	16.774	68.697
60-62	14.258	17.034	68.708
66-68	22.668	15.705	61.627
72-74	26.892	14.772	58.336
78-80	32.953	15.433	51.614
84-86	35.207	15.703	49.09
90-92	29.873	15.18	54.947
96-98	24.033	15.021	60.946
102-104	43.308	13.92	42.772
108-110	20.857	13.57	65.573
114-116	30.546	15.686	53.768
120-122	17.678	17.64	64.682
126-128	39.085	13.775	47.14
132-134	43.382	15.147	41.471
138-140	38.102	16.895	45.003
144-146	32.818	14.493	52.689
150-152	41.816	15.232	42.952
156-158	59.692	12.055	28.253
162-164	53.832	14.092	32.076
168-170	42.021	18.29	39.689
174-176	64.934	10.002	25.064
180-182	63.596	9.003	27.401
186-188	67.227	7.116	25.657
192-194	63.691	9.032	27.277
198-200	69.691	7.513	22.796
222-224	57.299	9.297	33.404
228-230	56.85	12.809	30.341
234-236	62.836	9.291	27.873
240-242	54.265	12.014	33.721
246-248	45.952	12.019	42.029
252-254	57.256	12.496	30.248
258-260	37.787	12.137	50.076
264-266	53.665	10.384	35.951
270-272	36.125	14.318	49.557

TM0503 VC2		
Interval	Percent Sand	Percent Mud
0-2	78	22
6-8	74	26
12-14	74	26
24-26	82	18
30-32	87	13
36-38	88	12
42-44	88	12
48-50	85	15
54-56	91	9
60-62	83	17
66-68	86	14
72-74	92	18
78-80	73	28
84-86	77	23
90-92	71	29
96-98	45	55
102-104	40	60
108-110	42	58
114-116	49	51
120-122	30	70
126-128	54	46
132-134	52	48
138-140	41	59
144-146	60	40
150-152	46	54

TM0503 VC13					
Interval	Percent Sand	Percent Mud	Percent Sand	Percent Silt	Percent Clay
0-2	13	87	14	14	73
6-8	10	90	11	14	76
12-14	18	82	16	16	67
18-20	5	95	6	17	77
24-26	7	93	9	17	75
30-32	10	90	11	17	72
36-38	13	87	15	24	61
42-44	14	86	14	20	66
48-50	14	86	15	23	62
54-56	22	78	22	20	58
60-62	23	77	23	18	60
66-68	31	69	29	16	55
72-74	39	61	36	15	49
78-80	36	64	33	17	50
84-86	35	65	33	17	50
90-92	12	88	-	-	-
96-98	20	80	18	20	62
102-104	19	81	16	18	66
108-110	18	82	16	17	67
114-116	9	91	11	25	64
120-122	11	89	12	16	72
126-128	24	76	25	11	64
132-134	18	82	17	12	71
138-140	13	87	14	9	77
144-146	9	91	14	9	76
150-152	34	66	32	12	56
156-158	38	62	36	8	57
162-164	26	74	25	6	69
168-170	61	39	48	4	47
174-176	51	49	42	6	52
180-182	58	42	52	6	42
186-188	39	61	50	7	43
192-194	72	28	63	6	30
198-200	64	36	55	11	34
204-206	58	42	-	-	-
210-212	57	43	-	-	-
216-218	54	46	-	-	-
222-224	36	64	-	-	-
228-230	45	55	-	-	-
234-236	44	56	-	-	-
240-242	24	76	-	-	-
246-248	23	77	-	-	-
252-254	20	80	-	-	-
258-260	15	85	-	-	-
264-266	17	83	-	-	-

270-272	26	74	-	-	-
276-278	16	84	-	-	-
282-284	53	47	-	-	-
288-290	11	89	-	-	-
294-296	28	72	-	-	-
300-302	30	71	-	-	-
306-308	29	71	-	-	-
312-314	23	77	-	-	-
318-320	29	71	-	-	-
324-326	22	78	-	-	-

TM0503 VC15					
Interval	Percent Sand	Percent Mud	Percent Sand	Percent Silt	Percent Clay
0-2	47	53	47	21	32
6-8	49	51	49	19	32
12-14	28	72	28	18	54
18-20	32	68	32	20	48
24-26	37	63	37	17	47
30-32	34	66	34	21	45
36-38	44	56	44	17	39
42-44	31	69	31	16	53
48-50	25	74	25	22	52
54-56	37	63	37	16	48
60-62	26	74	26	20	54
66-68	24	76	24	24	52
72-74	28	72	28	21	51
78-80	49	51	49	17	34
84-86	52	48	52	14	35
90-92	49	51			
96-98	53	47			
102-104	58	42			
108-110	64	36			
114-116	68	32			
120-122	62	38			
126-128	66	34			
132-134	78	22			
138-140	77	23			
144-146	79	21			
150-152	79	21			
156-158	73	27			
162-164	82	18			
168-170	82	18			
174-176	83	17			
180-182	79	21			
186-188	82	18			

192-194	82	18			
198-200	59	41			
204-206	82	18			
210-212	83	17			
216-218	85	15			
222-224	81	19			
228-230	87	13			
234-236	85	15			
240-242	82	18			
246-248	79	21			
252-254	75	25			
256-258	60	40			

TM0503 VC16
Summary of Settling Column Results

Depth Interval	Mean_gs (mm)	Sigma	Skewness	Kurtosis
15-17	176.23	0.5531	0.1324	9.4822
30-32	182.42	0.301	-0.736	49.4374
45-47	171.87	0.4592	0.9022	7.7715
45-47	159.63	0.6921	-2.9775	18.9596
60-62	167.17	0.5634	-2.5396	17.1597
75-77	176.87	0.4494	-0.7397	9.7602
90-92	174.5	0.7507	-1.2165	7.6906
105-107	199.15	0.4871	0.3871	2.7294
120-122	181.62	1.1001	-2.116	8.5699
135-137	219.04	0.4438	1.6501	-1.1183
140-142	194.68	0.6175	-0.0765	3.6323
155-157	177.59	0.48	-0.1947	6.3189
170-172	170.83	0.5818	-0.256	5.386
185-187	169.19	0.2568	59.7053	-773.64
200-202	140.29	0.3148	14.911	-84.934

TM0503 VC17			
Depth	Percent Sand	Percent Silt	Percent Clay
0-2	6	18	76
6-8	5	22	73
12-14	6	18	76
18-20	3	16	81
24-26	13	16	72
30-32	14	15	71
36-38	13	14	72
42-44	10	16	74
48-50	15	13	72
54-56	22	16	62
60-62	21	18	61
66-68	25	16	58
72-74	29	21	51
78-80	18	21	61
84-86	28	18	55
90-92	22	22	56
96-98	27	20	53
102-104	21	22	58
108-110	24	22	55
114-116	35	18	47
120-122	28	23	49
126-128	24	24	52
132-134	28	24	48
138-140	3	13	84
144-146	25	18	57
150-152	25	26	49
156-158	28	25	47
162-164	24	23	53
168-170	34	23	43
174-176	33	26	42
180-182	31	24	45
186-188	24	27	49
192-194	25	26	48
198-200	23	28	49
204-206	12	38	51
210-212	6	38	56
216-218	6	37	57
222-224	5	37	59
228-230	5	33	62
234-236	7	35	58
240-242	7	41	53

TM0503 VC18			
Interval	Percent Sand	Percent Silt	Percent Clay
0-2	25	20	55
6-8	34	19	47
12-14	39	7	54
18-20	37	10	53
24-26	41	11	48
30-32	40	8	52
36-38	48	8	44
42-44	41	9	50
48-50	38	10	51

TM0503 VC26					
Interval	Percent Sand	Percent Clay	Percent Sand	Percent Silt	Percent Clay
0-2	87	13	-	-	-
6-8	76	24	-	-	-
12-14	73	27	-	-	-
18-20	55	45	-	-	-
24-26	28	72	-	-	-
30-32	38	62	-	-	-
36-38	29	71	-	-	-
42-44	23	77	-	-	-
48-50	58	42	-	-	-
54-56	30	70	-	-	-
60-62	47	53	-	-	-
66-68	28	72	-	-	-
72-74	35	65	-	-	-
78-80	43	57	-	-	-
84-86	37	63	34	19	47
90-92	34	66	31	25	44
96-98	25	75	26	28	47
102-104	42	58	38	21	41
108-110	2	98	-	-	-
114-116	4	96	-	-	-
120-122	1	99	-	-	-
126-128	1	99	-	-	-
132-134	0	100	-	-	-
138-140	1	99	6	8	87
144-146	8	92	9	9	82
150-152	3	97	4	9	87
156-158	8	92	-	-	-
162-164	3	97	-	-	-
168-170	0	100	1	3	96
174-176	0	100	2	1	97

180-182	0	100	-	-	-
186-188	1	99	-	-	-
192-194	1	99	2	2	96
198-200	1	99	2	2	97
204-206	1	99	2	5	93
210-212	0	100	2	5	93
216-218	1	99	1	2	97
222-224	1	99	3	6	91
228-230	1	99	4	23	73
234-236	1	99	2	5	94
240-242	0	100	1	2	98
246-248	1	99	1	5	94
252-254	2	98	3	5	93
258-260	1	99	2	8	90
264-266	1	99	3	16	82
270-272	0	100	1	8	92
276-278	1	99	5	10	86

TM0503 VC28					
Interval	Percent Sand	Percent Clay	Percent Sand	Percent Silt	Percent Clay
0-2	3	97	3	15	82
6-8	4	96	4	11	85
12-14	5	95	6	8	86
18-20	3	97	3	8	88
24-26	6	94	6	11	82
30-32	8	92	8	22	70
36-38	11	89	11	34	55
42-44	8	92		-	-
48-50	7	93	7	22	71
54-56	4	96	9	30	62
60-62	6	94	6	10	85
66-68	3	97	3	15	82
72-74	1	99	1	15	84
78-80	1	99	2	6	93
84-86	2	98	3	8	89
90-92	2	98	3	15	82
96-98	1	99	2	6	91
102-104	1	99	2	5	93
108-110	3	97	3	8	89
114-116	8	92	17	2	81
120-122	23	77	23	5	72
126-128	24	76	24	5	72
132-134	20	80	23	5	72
138-140	38	62	38.05	9	53

144-146	62	38	-	-	-
150-152	69	31	-	-	-
156-158	67	33	-	-	-
162-164	75	25	-	-	-
168-170	70	30	-	-	-
174-176	75	25	-	-	-
180-182	82	18	-	-	-
186-188	65	35	--	--	--
192-194	63	37	-	-	-
198-200	66	34	-	-	-
204-206	79	21	-	-	-
210-212	76	24	-	-	-
216-218	56	44	-	-	-
222-224	51	49	-	-	-
228-230	57	43	-	-	-
234-236	66	34	-	-	-
240-242	66	34	-	-	-
246-248	59	41	-	-	-

Appendix B: Impact of Tropical Systems on the Sedimentary Fabric of the Mississippi Sound

VITA

Brian M. Velardo was born on October 2, 1978, in Baton Rouge, Louisiana. He graduated from his high school, Catholic High School of Baton Rouge, in May 1997. Following high school he enrolled in Louisiana State University and Agricultural and Mechanical College where he earned a Bachelor of Science degree in geology and geophysics in December 2001. Brian has been a fulltime graduate student at Louisiana State University and Agricultural and Mechanical College in the Department of Oceanography and Coastal Sciences since January 2002 and is presently a candidate for the degree of Master of Science in oceanography and coastal sciences.